AFRL-PR-WP-TR-1999-2078

STUDIES OF SURFACE DEACTIVATION OF VIBRATIONALLY-EXCITED HOMONUCLEAR MOLECULES IN GASEOUS DISCHARGE MEDIA USING COHERENT ANTI-STOKES RAMAN SPECTROSCOPY (CARS)

PERRY P. YANEY, PH.D.
JOHN W. PARISH

UNIVERSITY OF DAYTON
300 COLLEGE PARK
DAYTON, OH 45469

JANUARY 1999

FINAL REPORT FOR 04/01/1993 – 08/01/1998

PROPULSION DIRECTORATE
AIR FORCE RESEARCH LABORATORY
AIR FORCE MATERIEL COMMAND
WRIGHT-PATTERSON AIR FORCE BASE OH 45433-7251

NOTICE

When Government drawings, specifications, or other data are used for any purpose other than in connection with a definitely Government-related procurement, the United States Government incurs no responsibility or any obligation whatsoever. The fact that the government may have formulated or in any way supplied the said drawings, specifications, or other data, is not to be regarded by implication, or otherwise in any manner construed, as licensing the holder, or any other person or corporation; or as conveying any rights or permission to manufacture, use, or sell any patented invention that may in any way be related thereto.

This report is releasable to the National Technical Information Service (NTIS). At NTIS, it will be available to the general public, including foreign nations.

This technical report has been reviewed and is approved for publication.

BISWA N. GANGULY
Power Systems Branch
Power Division
Propulsion Directorate

JOHN C. HORWATH
Acting Chief, Power Systems Branch
Power Division
Propulsion Directorate

JERRY E. BEAM
Acting Chief
Power Division
Propulsion Directorate

If your address has changed, if you wish to be removed from our mailing list, or if the addressee is no longer employed by your organization please notify AFRL/PRPS, Wright-Patterson AFB, OH 45433-7919 to help us maintain a current mailing list.

Copies of this report should not be returned unless return is required by security considerations, contractual obligations, or notice on a specific document.

REPORT DOCUMENTATION PAGE	Form Approved OMB No. 0704-0188

1. AGENCY USE ONLY *(Leave blank)*	2. REPORT DATE	3. REPORT TYPE AND DATES COVERED
	JANUARY 1999	FINAL REPORT FOR 04/01/1993 - 08/01/1998

4. TITLE AND SUBTITLE
STUDIES OF SURFACE DEACTIVATION OF VIBRATIONALLY-EXCITED HOMONUCLEAR MOLECULES IN GASEOUS DISCHARGE MEDIA USING COHERENT ANTI-STOKES RAMAN SPECTROSCOPY (CARS)

5. FUNDING NUMBERS
C F33615-93-C-2303
PE 61102
PR 2301
TA P1
WU 01

6. AUTHOR(S)
PERRY P. YANEY, PH.D.
JOHN W. PARISH

7. PERFORMING ORGANIZATION NAME(S) AND ADDRESS(ES)
UNIVERSITY OF DAYTON
300 COLLEGE PARK
DAYTON, OH 45469

8. PERFORMING ORGANIZATION REPORT NUMBER
UDR0001Z

9. SPONSORING/MONITORING AGENCY NAME(S) AND ADDRESS(ES)
PROPULSION DIRECTORATE
AIR FORCE RESEARCH LABORATORY
AIR FORCE MATERIEL COMMAND
WRIGHT-PATTERSON AFB, OH 45433-7251
POC: BISWA N. GANGULY, AFRL/PRPS, 937-255-2923

10. SPONSORING/MONITORING AGENCY REPORT NUMBER
AFRL-PR-WP-TR-1999-2078

11. SUPPLEMENTARY NOTES

12a. DISTRIBUTION AVAILABILITY STATEMENT
APPROVED FOR PUBLIC RELEASE, DISTRIBUTION UNLIMITED.

12b. DISTRIBUTION CODE

13. ABSTRACT *(Maximum 200 words)*

SEE REVERSE

14. SUBJECT TERMS
Nitrogen, Wall relaxation rate, Heterogeneous deactivation coefficient, Coherent anti-Stokes raman spectroscopy, CARS, Vibrational deactivation rates of nitrogen X state

15. NUMBER OF PAGES
59

16. PRICE CODE

17. SECURITY CLASSIFICATION OF REPORT	18. SECURITY CLASSIFICATION OF THIS PAGE	19. SECURITY CLASSIFICATION OF ABSTRACT	20. LIMITATION OF ABSTRACT
UNCLASSIFIED	UNCLASSIFIED	UNCLASSIFIED	SAR

Standard Form 298 (Rev. 2-89) (EG)
Prescribed by ANSI Std. 239.18
Designed using Perform Pro, WHS/DIOR, Oct 94

ABSTRACT

Deactivation coefficients, γ_v, of vibrationally-excited $N_2(X^1\Sigma_g^+,v)$ on alloys of aluminum, stainless steel alloys, a titanium alloy, gold, Pyrex glass and Teflon were determined from measurements of the wall deactivation rate, k_v, for the v = 1 to 4 or 5 hot bands using coherent anti-Stokes Raman spectroscopy (CARS). A water-cooled positive column discharge was used to populate the vibrational states. The nitrogen gas flow rate was adjusted to optimize the observed decay of the populations. The excited gas was exposed to the tubular specimen surface for precisely controlled residence times and efforts were made to track the influence of surface properties. The BOX CARS configuration was used to spatially resolve only the gas that was exposed to the specimen surface. Extensive measurements on Pyrex gave γ_1 values between 2.4×10^{-4} and 6.7×10^{-4} depending on the treatment history of the surface. The values for γ_4 ranged from 2.9×10^{-4} for the AMS 4943D alloy of titanium to approximately unity for the AMS 312 stainless steel alloy. The low value for titanium can be attributed to the oxide layer. The observed values for gold decreased with increasing temperature consistent with a physical adsorption process. For nearly all specimens, k_v was proportional to v, or nearly so. Moreover, γ_v values for neat Pyrex, gold foil and aluminum showed similar proportional dependencies on v.

TABLE OF CONTENTS

INTRODUCTION

Vibrationally excited molecules play various roles in gas kinetics and plasma chemistry. Of the seven diatomic, homonuclear molecules occurring at normal temperatures, nitrogen holds interest due to its importance in combustion, biology, microelectronics, high speed and high altitude aircraft and spacecraft reentry. Vibrational energy in the ground electronic state of nitrogen is important in the short-lived pink afterglow production where Penning ionization and the rapid e-V exchange leads to considerable heat loss and $N_2(B^2\Sigma_u^+)$ pumping.[1] Vibrational energy is important in promoting plasma chemistry where it is an available energy source for molecular dissociation. Here radicals or atoms are delivered where needed as in plasma-enhanced chemical vapor deposition (PECVD).[2] Published research into the catalytic chemistry of active nitrogen in low pressure post-discharge gas revealed the presence of a large concentration of excited ground state nitrogen $N_2(X^1\Sigma_g^+, v)$ accompanying $N(^4S_{3/2})$ atoms.[3] Accurate calorimetric measurements of atom recombination require correction for the vibrational energy deposition. Accurate theoretical models of vibrational distribution require specific state-selective measurements, which have been developed.[4,5]

Vibrational energy transfer of $N_2(X^1\Sigma_g^+, v)$ to solid surfaces is addressed in this work. Population distributions and loss rates in the presence of a surface were studied. These results extend the knowledge about diatomic molecular wall loss rates to higher v-states than is currently available. This information can influence the design of gas lasers and improve our understanding of all reactive gaseous environments, such as in combustors, in plasma processing chambers for microelectronics and on high temperature exterior surfaces of high speed aircraft. In this work, vibrationally excited nitrogen was exposed to tubular reactor surfaces of common construction materials. This list includes neat Pyrex, Pyrex exposed to active nitrogen, type 3003 aluminum, types 304 and AMS 312 stainless steel, AMS 4943D titanium, 99.999% pure gold and Teflon. The tubular reactor elements had an internal diameter of about 1.5 cm and were cut into specimens about 12 cm long.

A flowing afterglow created in a water-cooled, dc electric discharge reacted with each surface for precisely-stepped residence times. The glow discharge provided a low translational temperature and a high vibrational excitation with insignificant atom and charged species densities. This gave spectra which had isolated vibrational bands with significant rotational line intensities limited to approximately J = 21. The vibrational wall deactivation rates were measured for the v = 1 to either the v = 4 or 5 vibrational "hot" bands by probing the axial flow with a small-volume optical probe using coherent anti-Stokes Raman spectroscopy (CARS). Although signals from the v = 6 band were observed, useful measurements above the v = 5 band were virtually impossible under our conditions. In essence this means those populations were too small to have an impact on the experiment as a whole. Nonequilibrium distributions were characterized by rotational temperatures of ~350 K and vibrational temperatures of ~2000 K. Numerous experiments were made on some surfaces to determine repeatability. At the same time, a slow change in the surface due to the afterglow was observed for every surface. Measurements were made on the axis of the gas flow and referred to the surface by calculation.

Observed deactivation rate k_v, which include both homogeneous and heterogeneous deactivation, and the "apparent" deactivation coefficients γ_{va} for the surfaces are reported for each measured $v \rightarrow v + 1$ band. The vibrational distribution in the bulk of the gas depends on the deactivation rates and radial diffusion. Relaxed molecules must diffuse to the probe volume before the effect can be seen. Moreover, the observed deactivation due to the surface is significantly modified by the fast vibrational-vibrational (V-V) exchange processes via diffusion. These processes soften the effect of wall deactivation by the redistribution of the populations up the vibrational energy level ladder. This process is strong when there is significant populations in the low-lying vibrational levels such as produced by a gaseous discharge. For the low lying v-levels studied here (≤ 5), the vibrational-translational (V-T) exchange rates are insignificant. In order to extract the "true" wall deactivation rates $k_{v(wall)}$ from k_v, a Master Equation Model of N_2 was fitted to the data for four specimens with the $k_{v(wall)}$ as fitting parameters. This model includes V-V and V-T energy exchange processes as well as wall exchange interactions. It uses the Schwartz-Slawsky-Herzfeld (SSH) law of

scaling deactivation rates and the development of the model closely follows that of Bailey[6] and Capitelli.[7] From this procedure, "true" values of $k_{v(wall)}$ and γ_v were determined. As described in a later section, this fitting effort was greatly complicated by the fact that the model computed populations out to v = 40 while data was available only up to v = 4 or 5. This required an extrapolation procedure to constrain the fitting of the populations above v = 4 or 5. It was found that many of the data sets could not be adequately constrained to permit unambiguous fittings. Nevertheless, it is suggested that the four successful fittings provide information that can be used to provide reasonable corrections of the γ_{va} for all the specimens to viable estimates of the "true" γ_v.

The Experimental Details section describes the gaseous discharge system and the procedures used to establish a clean gaseous system. The CARS optical system and the electronic data acquisition system are also described. The Theory section reviews the basic characteristics of the CARS technique and gives a detailed analysis of the dependence of the deactivation coefficient measurements on the observed deactivation rate and diffusion. A review of the Master Equation Model is also included. The data collection procedures, the corrections for stimulated Raman scattering and the normalization procedures are presented in the Analysis section. This section also includes the procedure used to measure the peak values of the rotational lines and the method use to unfold the population decay rates of the individual v states from the population differences obtained form the CARS data. The Data and Results section reports the results of all the deactivation measurements including the fitting results using the Master Equation Model. The results of the XPS measurements on selected specimens are reported here also.

EXPERIMENTAL DETAILS

In an experimental apparatus similar to that used by Black et al.,[8] the vibrationally-excited molecules, generated in the low pressure dc discharge, were carried in the afterglow through a 15-cm-long tubular reactor in which diffusion carried them to the surface. Black et al. used mostly a thermal source and a 100-cm-long reactor. Because of this long flow tube length, they had to correct for Poiseuille flow. Moreover, they could only achieve sufficient excitation to observe the $v = 1 \rightarrow 0$ transition using spontaneous anti-Stokes Raman scatttering. A fraction γ_v of the excited molecules which collide with a surface having a catalytic capability result in the transfer of vibrational energy to the surface vibrational modes.[9] The population distribution remaining in the gas was measured after stepped residence times of contact of the gas with the surface. The pressure chosen for these measurements was typically between 10 and 20 Torr. This pressure was sufficient to provide adequate CARS signals and low enough to permit efficient steady state production of vibrationally-excited nitrogen in the discharge. From the observed decay of the vibrational populations with time, the total rate coefficients k_v were determined from which the apparent wall deactivation efficiencies γ_{va} were calculated for each vibrational level. The total rate coefficients are independent of the size of the probe volume as well as the radial location in the tubular specimen. They do depend, however, on the combined effects of collisions with the surface and the gas-gas collisions. For the conditions of these studies, the latter is dominated by V-V processes. For given values of "true" γ_v, the observed rate coefficients k_v depend on the temperature, pressure and tube radius. The γ_v, however, are characteristics of the surface which are determined by surface activity, temperature, the colliding molecule, and possibly pressure. By fitting the Master Equation Model to these population data, extraction of $k_{v(wall)}$ free of homogeneous effects was attempted. However, because the coupled equations are stiff and the fitting process is highly dependent on the fact that the rate

of change of population in one level is highly coupled to neighboring populations via the V-V processes, this effort gave viable results only for certain data sets.

A flowing gas handling system carried nitrogen (Air Products ultra-pure carrier grade 99.999% pure) through a water-cooled dc electric discharge operating in the range of 11 to 22 Td with 40 cm of the positive column exposed to the flow. The flowing afterglow passed around a right-angle bend and then through the tubular reactor specimen. Tylan General FC-260 flow controllers maintained steady mass flow to in the range of 0 to 2000 sccm calibrated to within 0.2%. The gas supply system was all stainless steel except for the Pyrex discharge tube, the source tube (which carried the active nitrogen to the specimen tube) and a 0.8 m section of flexible polyethylene tubing at the input of the discharge tube which prevented the plasma from striking up-stream. The experiments were accomplished between 11 and 23 Torr (67 to 3066 Pa) with most measurements at 14 Torr. In Fig. 1, the positive column discharge pumps the vibrational states to nonequilibrium. The vibrational temperature of the gas entering the specimen tube, T_v, ranged from about 1800 to 2800 K while the gas temperature, T_g, was between about 315 to 380 K. Either a dc discharge or a cw microwave source could have been used to preferentially pump $N_2(X,v)$.[10] The dc discharge avoided high concentrations of $N(^4S)$ atoms and N_2 B- and A-state molecules. Recombination of the residual atom concentration produced the weak straw-colored Lewis-Rayleigh afterglow.[1,11] A spectroscopic study of this $N_2(B \rightarrow A)$ glow with residence time provided a measure of atom recombination on the wall and in the gas and gave a rough estimate of N density.[12] The mole fraction of N atoms was found to be about 0.0055. The transit time of the gas in the source tube was no less than 20 ms. This insured that the density of electronically-excited molecules was at least two orders of magnitude less than the N atom density and thus a small fraction of the observable $N_2(X,v)$ populations of the gas impacting the specimen surface. Moreover, all charged species had sufficient time to become neutralized well before they came in contact with the specimen surface.

Exiting the discharge, the gas turned 90 degrees, past a Wood's horn, into the source tube where a pink afterglow terminated. The line-of-sight from the discharge tube terminated into the Wood's horn in order to prevent near-UV emissions from the plasma exciting the gas

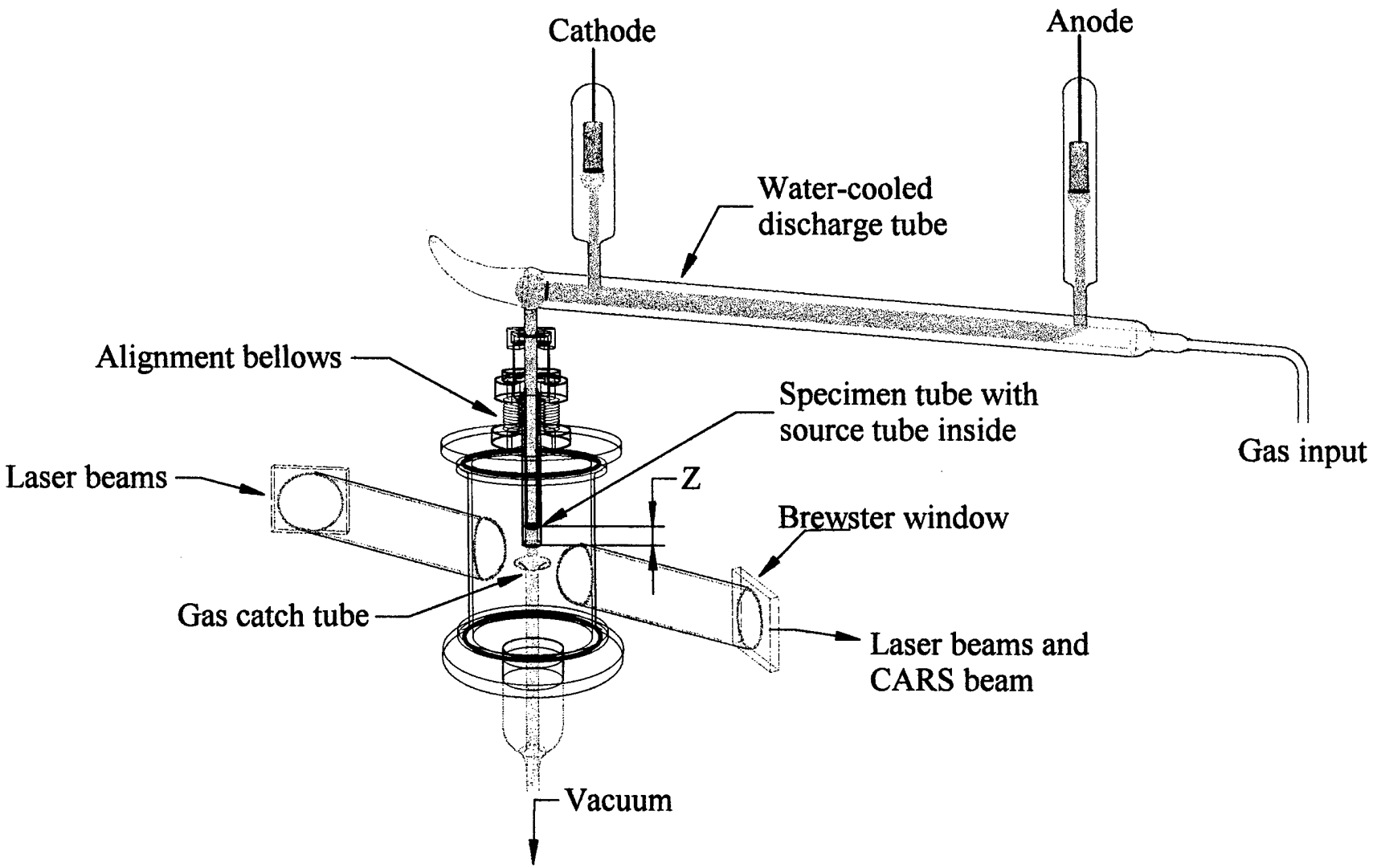

Figure 1. Diagram of discharge tube and probe chamber for measuring deactivation rates as a function of Z.

entering the reactor specimen tube. During the transit to the specimen tube, the gas cooled and attained steady state conditions giving a steady population at the exit of the source tube. The position of the source tube, which was sealed through an O-ring gland in the top of the optically-accessible main chamber, could be positioned to ±0.1 mm, providing very accurate control of the residence time of the gas in the specimen tube. Brewster-angle windows were mounted on 15-cm-long tubular extensions on the chamber which permitted focusing of the high peak-power CARS beams in the chamber without damaging the windows. There was also a pair of side windows for emission experiments. The CARS signals were generated by probing the gas along a diameter through the axis of the specimen tube in a 1-cm gap between bottom of the specimen tube and the top of the gas "catch" tube. The catch tube was connected to a vacuum pump through a set of three valves arranged to provide for on/off, coarse and fine control of the pumping rate on the main chamber. Pressure was regulated by manual butterfly and needle valves some 150 cm distance after the specimen tube and monitored with a pair of Wallace and Tiernan gauges (0 to 20 and 0 to 200 Torr absolute) connected to the main chamber. Additional 6-mm-diameter gas outlets in the floor of the main chamber constrained recirculation of the gas. A computer-generated analog signal controlled the mass flow controller. Thermocouple and Convectron gauges were incorporated for base pressure and helium leak checking of the system, respectively.

At more than a meter upstream of the discharge tube, a mixing chamber that had three inlet ports was used to mix nitrogen with argon or helium as needed. The system was returned to atmospheric pressure with pure nitrogen or argon. Before each experiment, each specimen was degreased with methylene chloride in a sonic cleaner before insertion in the main chamber. The source and specimen surfaces were cleaned with an argon discharge around 2 Torr at 60 mA. The pressure was varied between 0.25 and 10 Torr during this procedure to promote out-gassing of any trapped gases. No oxygen or water could be detected in gas samples taken from the system and analyzed locally by Fourier transform mass spectrometry.[13] The supply and exhaust systems were periodically baked out assisted by a combination of heat tapes and heat gun with either flowing gas or pumping at the 1 μm base pressure for six to eight hours. Base pressure was accomplished with an isolated secondary

system including an Edwards mechanical pump fitted with a molecular sieve at the inlet port. The primary flow system was pumped by a Welch mechanical pump fitted with an oil mist filter and vented outside the lab. At no time were primary and secondary pumps operated together. Moreover, the primary pump was never opened at or below its base pressure of 25 μm and was always operated with flowing gas.

Mass flow was regulated to a fixed value for each experiment between 450 and 1200 sccm ±0.2%. This provided an axial transport speed between about 2 and 8 m/s in the specimen tube. This gave from 15 to 60 ms maximum residence time of the vibrationally active gas in the specimen tube and more than 20 ms in the source tube. Because the specimen tube length-to-diameter ratio was small (≤8), plug flow was assumed, thereby requiring no correction for Poiseuille flow.

CARS is an effective probe of ground electronic state vibrational levels in homopolar diatomic molecules. Lack of a vibrational-rotational absorption spectrum due to the absence of electric dipole transitions compels the use of a Raman probe. At low pressures the nonlinear process produces little signal generation advantage over linear Raman spectroscopy; however, the nonlinear process generates a signal that is confined to a coherent beam which greatly simplifies the signal collection. On the other hand, two complications demand careful attention. The change in the third order, nonlinear susceptibility in the CARS process is proportional to the difference between the populations of the two quantum levels probed by the laser beams. This requires an analysis step, discussed in the Analysis section, that extracts fractional populations from signal data containing population differences. Secondly, stimulated Raman scattering (SRS) simultaneously pumps population from the lower to the upper level, which introduces a laser-power-dependent systematic shift in the signal measurements. This "saturation" effect has been the subject of an investigation similar to studies reported here.[14] However, it was necessary to independently determine the correction for the intermediate peak laser power levels used in these studies.[15] This correction requires a calibration step which is briefly described in the Analysis section.

The pulsed lasers used in the CARS system consisted of an injection seeded, doubled Spectra-Physics DCR-3 Nd:YAG laser which pumped a Lumonics HyperDye 300 tunable dye

laser. The YAG laser produces a 7 ns pulse and provided a CARS pump beam at 532 nm with a single longitudinal mode linewidth of 0.006 cm^{-1} (0.00017 nm, 180 MHZ). The dye laser, using sulforhodamine 640 dye, produced a 5 ns, multimode CARS probe beam with a linewidth of 0.1 cm^{-1} (0.0037 nm, 3 GHz) over the range of 16,640 to 16,390 cm^{-1} (601 to 610 nm). It was found that 22.33 mg dye per liter methanol dilution provided a slowly varying power curve over this range. Figure 2 is a diagram of the optical system used in this work. The figure shows how the appropriate timing delay of the YAG beams was accomplished through a series of prisms. The YAG and dye laser beam energies were adjusted using half-wave plates in combination with polarizing prisms.[16] The main pump beam was split into two equal-energy, parallel beams about 2 cm apart with a beam-splitter mirror and aligned symmetrically on the focusing lens. The probe beam was increased in diameter through a beam-expanding telescope in order to approximately match the dye beam waist to the waist sizes of the two pump beams in the focal volume of the lens. The probe beam was aligned in a plane perpendicular to the plane of the pump beams so as to satisfy the BOX CARS phase matching condition.[17] The pump beams were elliptical in cross section with major and minor axis dimensions at full width at half maximum (FWHM) of 300 μm and 100 μm, respectively. The waist diameter of the dye beam was 70 μm FWHM. These dimensions were determined by knife-edge test and burn patterns. The length of the overlap or probe volume of the three beams was measured to be about 5 mm by translating a thin argon sheet through the volume while measuring the air signal. The tolerance on the positioning of the probe volume was ±2 to 3 mm due to the length of the probe volume and the 15-mm tube diameter. This positioning was accomplished by translating the main chamber parallel to the probe beams while measuring the CARS signal for the v = 1 to 2 transition. Beam alignment was checked before each experiment by peaking the ~473-nm CARS signal with the dye beam focusing lens. During chamber maintenance, beam crossing alignment was achieved by passing the three attenuated beams through a pin hole. The BOX CARS beam arrangement was chosen because it permitted precise location of the measurement volume. A scheme using 60° rotated polarization in each beam, available for suppressing the nonresonant background, was not used because the signal is reduced by one third.[18] Since the nonresonant background in these measurements was very weak, this signal reduction was deemed too great considering the

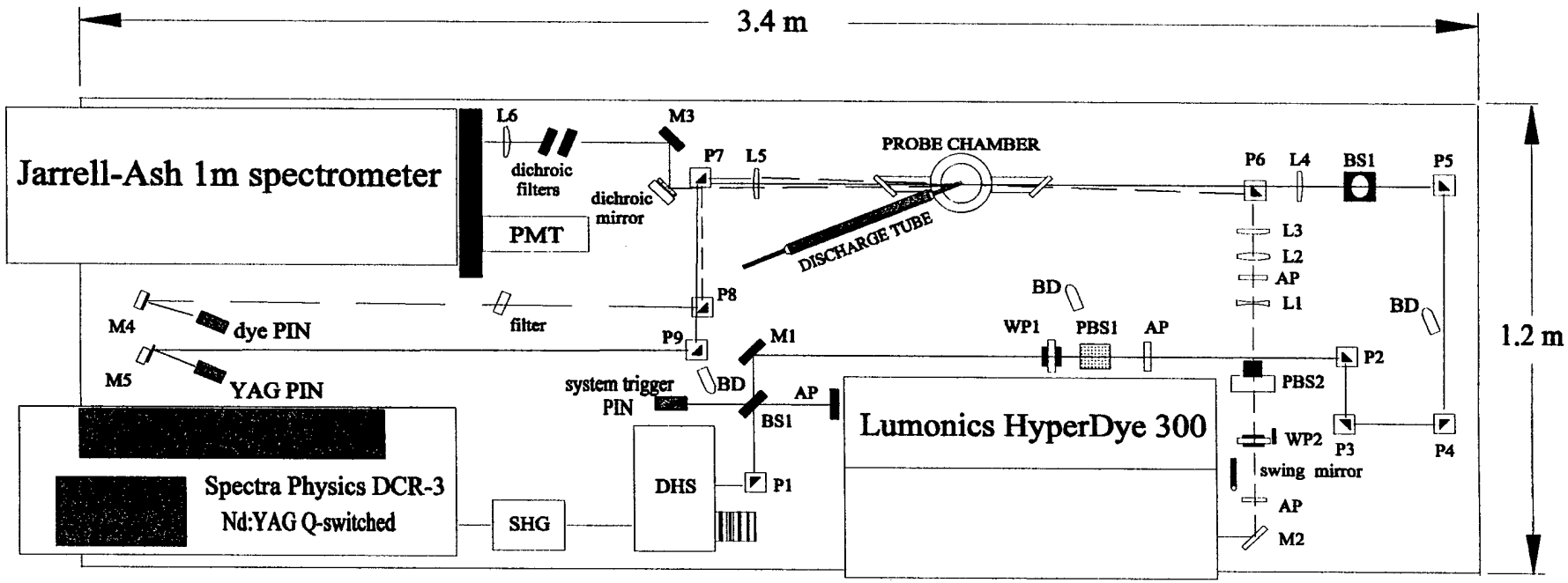

Figure 2. CARS optical system used in measuring the deactivation rates. Labels: AP, aperture; BD, beam dump; BS#, beam splitter; DHS, dichroic harmonic separator; L#, lens; M#, mirror; P#, prism; PBS#, polarizing beam splitter; PIN, photodiode; PMT, photomultiplier; SHG, second harmonic generator; WP#, half-wave plate.

diminutive size of the signals from the low pressure gas. All beams were horizontally polarized parallel with the optical table.

Beam powers incident on the main chamber were tracked with PIN diodes calibrated between each run within each experiment. Diode counts linearly tracked the incident fluence and systematic energy deviations in the laser pulses. While the diode signal counts were proportional to the incident pulse energy, average power measurements were more convenient to use because the average diode signal was used in normalizing the average CARS signal. These diodes were an important nexus between saturation calibration and the deactivation experiments. The count-to-mW ratios of each deactivation experiment and the associated saturation calibration experiment were used to convert the power in the deactivation measurements to the equivalent power used in the saturation measurements. The degree of saturation S was then calculated and returned to correct the raw CARS signal values.

Instead of using a high pressure argon gas cell to reference the measurements, which was really impractical for our system besides being notoriously difficult to keep aligned, the averages of the outputs of the laser PIN diodes were used to normalize the CARS signals. These integrated signals tracked power changes in the two beams within a run as well as between runs within an experiment. During any given deactivation or saturation run, the standard deviation of the mean of the output of the YAG laser over 200 pulses was well under 1%. Due to mode beating in the dye laser, there was no significant correlation between the fluctuations in the dye laser output and the YAG laser output. Thus, assuming that there was no significant correlation between the susceptibility fluctuations and the dye laser fluctuations, the normalization of the CARS signal was accomplished by dividing the average CARS signal by the individual averages of the laser diode signals. The normalization and saturation correction are detailed in the Analysis section. In addition, signal changes due to the dye spectral power curve were removed initially by calibrating the wavelength response of the dye laser PIN diode. It was found subsequently that the combined spectral response of the receiver optics, spectrometer and photomultiplier tube (PMT) was flat over the operating range and needed no correction.

The receiver optics consisted primarily of a 500-mm-focal-length planoconvex lens, a right-angle prism for spatial separation of signal and laser beams, two p-polarization dichroic mirrors, two p-polarization dichroic filters, and a 39-mm, best-form lens for imaging the CARS beam on the entrance slit of a 1-m Jarrell-Ash grating spectrometer. The spectrometer was used primarily as an additional filter for rejection of any pump beam leakage light. An EMI 9816KB PMT performed CARS signal detection typically operating at 2100 V. The rejected beams were directed to beam dumps except for about 4% reflected from the hypotenuse of two prisms toward the PIN diodes.

Data acquisition and dye laser tuning was computer controlled through a Keithley Data Acquisition System Model 570. The data acquisition and control (DAqCt) software is written in GW BASIC which incorporates Keithley Soft500 BASIC libraries for controlling the Keithley 570. The final DAqCt program version, named SB9.BAS, consists of three separate programs: SB9, SB9KL1 and SB9KL2. This software has several features including the capability for manually controlling the dye laser and the flow controllers, automatically tuning the dye laser from a script file and carrying out the acquisition of a continuous spectrum or a skip spectrum from a script file.

Gated detection of the PMT and PIN diode signal pulses was used to minimize background signals and noise from ambient light and from radio frequency interference generated primarily in the YAG flash lamp power supply. The system trigger pulse was generated by a PIN diode from the YAG pulses which leaked through a turning mirror following the beam splitter for the dye laser. This trigger pulse was sent to a LeCroy Model 821 Discriminator to generate a NIM standard pulse which triggered a Hewlett-Packard (H-P) Model 3012B pulse generator. The output from this generator was attenuated and split into a clock start pulse and three -1.6-V gate pulses, each 70 ns long. The gate pulses provided the gating of the LeCroy Model 2249SG fast pulse analog-to-digital converter (ADC). The ADC digitized the integrated signal pulses from the PMT (i.e., the CARS signal) and the PIN diodes for the YAG and dye lasers. These signal pulses were appropriately delayed with coax delay cables such that they arrived at the ADC within the gate pulses. Each pulse was passed first through a 10-step Phillips Scientific Model 771 pulse amplifier. The gain was set to maximize the utilization of the ADC's 1000-count dynamic range so that

the maximum pulse did not exceed the dynamic range. The CARS signal was additionally attenuated using a motor-controlled neutral density filter wheel mounted in front of the PMT. This was necessary because of the more than 1000 to 1 range of the CARS signals. Both the amplifiers and the neutral density filters were calibrated to accuracies better than 0.1%. The YAG laser pulse noise level of 1% relative standard deviation was the lowest of the three signals. The dye laser presented about 4% to 6% noise while the noise on the CARS signal was typically between 22 to 33% relative standard deviation. Each laser PIN diode had an adjustable optical attenuator that greatly alleviated spatial alignment requirements and removed channel spectra in the dye diode. The attenuators consisted of a pair of telescoping brass tubes with an opal glass window at the interior end of each tube.

A fifth pulse from the first H-P pulse generator triggered a second H-P 3012B pulse generator which produced a 2.3 ms pulse for gating the Keithley 570. The computer reads the ADC after each laser pulse as many times as was programmed for that deactivation data point. After each data point, the program totaled the data and stored the value in a file. The wavelength was stepped and the process repeated. Later, the average signal values and uncertainties were then calculated.

The water cooling of the nitrogen glow discharge tube kept the gas temperature at the specimen tube below 400 K. This discharge tube was connected to a manually-operated, high voltage dc power supply through a high-power 50 kΩ ballast resistor. Typical voltages were about 8.8 kV at the power supply giving about 4.3 kV at the discharge terminals. The discharge current was set to 90 mA and monitored periodically throughout the experiment. Hollow Kovar electrodes were used in the discharge tube.

THEORY

CARS Probe Technique

The CARS technique was originally developed for the combustion community. Combustion is often accompanied by fluorescence emissions, high luminous emissions due to soot formation, high temperatures, chemical reactivity, turbulence and sometimes high transport velocities. Physical probes can disturb the chemistry or the population distributions, they are not generally state selective and they may be unable to physically survive the environment. An optical probe can overcome many of these difficulties. CARS has the highly-desired property of producing a large, coherent optical signal beam on the short wavelength side (i.e., blue side) of the incident laser wavelength thereby removing the signal from the strong, potentially interfering fluorescence and incandescence emissions that are on the red side of the laser wavelength. These emissions are typically generated when a laser beam is incident on a complex combustion medium. This is in contrast to the spontaneous Raman or laser-induced fluorescence techniques wherein the signals are usually on the red side of the laser wavelength. These techniques also have the disadvantage of requiring signal detection over a significant solid angle which introduces spatial resolution restrictions and limitations of use on highly luminous media. CARS has the disadvantages of requiring two optical ports that can withstand high peak power, short optical pulses and a limiting sensitivity of roughly one part per thousand (10^{16} cm^{-3}) in atmospheric flames. Under the conditions of the experiments reported here, the number density was almost two orders of magnitude below the value at atmospheric pressure and ranged over nearly 3.5 orders of magnitude which brings the lower limit to no more than 10^{14} cm^{-3}. There are several appropriately named variants of the technique depending on the geometry of the three input beams. A review of these is given in Eckbreth.[18] General reviews of the CARS technique can also be found in Arnold et al.,[19] Tolles,[20] Druet[21] and Attal-Tretout.[22] The essential characteristics of the technique are presented here.[23]

The CARS process is governed by a fourth-order susceptibility tensor, and thus is a member of the nonlinear family of four-wave mixing processes. The polarization *P(t)* of a

scattering medium is related to an incident electric field $E(t)$ by the relation $P(t) = \varepsilon_0 \chi E(t)$, where χ is the electric susceptibility of the medium and ε_0 is the permittivity of free space. Expanding the polarization in a power series one obtains

$$P(t) = \epsilon_0[\chi^{(1)}E(t) + \chi^{(2)}E^2(t) + \chi^{(3)}E^3(t)] \qquad (1)$$

where the $\chi^{(n)}$ factors are tensors of order n + 1. In four-wave mixing, the total applied field is made up of three incident fields that can be written as

$$E(t) = \frac{1}{2}[E_1(\omega_1)e^{-i\omega_1 t} + E_2(\omega_2)e^{-i\omega_2 t} + E_3(\omega_3)e^{-i\omega_3 t} + c.c.] \qquad (2)$$

where $E_i(\omega_i)$ is one of the incident plane waves of frequency ω_i, and the propagation directions are parallel. All three terms in Eq. (1) can, in general, be simultaneously nonzero. In a gas, however, the $\chi^{(1)}$ term describes Rayleigh scattering of the incident waves and $\chi^{(2)}$ vanishes identically. Substituting Eq. (2) into the $\chi^{(3)}$ term of Eq. (1), the general expression for the four-wave mixing polarization can be written

$$P_i(\omega_4=\omega_m+\omega_n+\omega_o)=\epsilon_0 \sum_{jkl} \sum_{(mno)} \chi^{(3)}_{ijkl}(\omega_4;\omega_m,\omega_n,\omega_o)E_j(\omega_m)E_k(\omega_n)E_l(\omega_o) \qquad (3)$$

where (mno) indicates the sum over the frequency components is restricted to the condition indicated in the polarization argument. The number of separate elements in $\chi^{(3)}_{ijkl}$ is 81. The number of elements that are actually needed is determined by symmetry properties of the probed medium. For an isotropic medium like a gas, there are 21 nonzero elements that possess the property that any Cartesian component which appears at least once must appear an even number of times. Thus, because of the equivalence of the three coordinate axes, the only surviving elements are xxxx, xxyy, xyxy, xyyx where xxxx = xxyy + xyxy + xyyx, which

specifies the polarizations of the four fields. In the experiments reported here, the polarizations of the incident fields were parallel corresponding to the xxxx component.

The terms of Eq. (3) of interest here are of the type given in Eq. (4), where the first expression corresponds to the case where there are two different pump waves at ω_1 and ω_2 with the probe wave at ω_3. The second and third expressions are essentially the same with $\omega_2 = \omega_1$. (Note that the ½ factors are not shown on the right sides of these expressions.)

$$\begin{aligned} P(\omega_4 = \omega_1 + \omega_2 - \omega_3) &= 6\chi^{(3)} E_1 E_2 E_3^* \\ P(\omega_4 = 2\omega_1 - \omega_3) &= 3\chi^{(3)} E_1^2 E_3^* \\ P(\omega_4 = 2\omega_2 - \omega_3) &= 3\chi^{(3)} E_2^2 E_3^* \end{aligned} \qquad \textbf{(4)}$$

In the case where two incident frequencies, one for a pump, $\omega_p = \omega_1$ or ω_2, and the other for the probe, $\omega_s = \omega_3$ (Stokes), corresponds to the resonance condition of $\omega_v = \omega_p - \omega_s$, where ω_v is the transition energy between two vibrational-rotational levels of nitrogen, then the number of terms contributing to the same interaction reduces to the 12 terms summarized in Eq. (4). If the expression for the electric field is written with both the temporal and spatial parts, where $\vec{k}_i$ are the propagation vectors, then

$$\vec{E}(\omega_i, \vec{r}) = \frac{1}{2} E_0 \exp(-i\omega_i t) \exp(i\vec{k}_i \cdot \vec{r}) + c.c. \qquad \textbf{(5)}$$

Substituting into Eq. (4) with $\omega_2 = \omega_1 = \omega_p$, the spatial phase of the coherent scattered wave, called the anti-Stokes wave, at frequency $\omega_4 = \omega_{as}$ becomes

$$\vec{k}_{as} \cdot \vec{r} = (2\vec{k}_p - \vec{k}_s) \cdot \vec{r} \quad .$$

If the incident waves are planar with $\vec{k}_p$ *and* $\vec{k}_s$ parallel and directed in the z direction, the signal wave will experience growth in this direction at the frequency $\omega_{as} = 2\omega_p - \omega_s$. Substituting Eqs. (4) and (5) into the wave equation, applying the slowly varying wave approximation and defining the phase mismatch $\Delta k = 2k_p - k_s - k_{as}$, one obtains

$$2ik_{as}\frac{\partial E(\omega_{as},z)}{\partial z} = -\frac{\omega_{as}^2}{c^2}\chi^{(3)}E^2(\omega_p)E^*(\omega_s)\exp(i\,\Delta k\,z) \qquad (6)$$

Integrating Eq. (6) over z = 0 to ℓ, squaring the result to obtain intensity and using

$$I_i = \frac{n_i\,c\,\epsilon_0}{2}|E(\omega_i)|^2 \qquad (7)$$

for each field, where n_i are the refractive indices and c is the speed of light, the expression for the CARS signal beam intensity can be written

$$I_{as} = \frac{\omega_{as}}{n_p^2 n_s n_{as} c^4 \epsilon_0^2} I_1^2 I_2 |\chi_{CARS}|^2\,\ell^2 sinc^2(\tfrac{1}{2}\Delta k\,\ell). \qquad (8)$$

where χ_{CARS} is the third order susceptibility for the CARS process. Maximum signal is achieved when the phase matching condition $\Delta k = 0$ is satisfied. It should be pointed out that the pump intensity is on the order of 1 GW/cm^2 in practice and the probe beam is weaker by a factor of roughly 10 but provides the coupling to the resonance properties of the medium. The strength of the CARS signal for given peak intensities of the pump and probe beams depends on the square of the CARS susceptibility, χ_{CARS} , which is proportional to the spontaneous Raman cross section times the difference in the population densities of the two levels connected by the process.

Diffusion and the Wall Loss Flux

The probability of losing vibration quanta from nitrogen molecules to a surface was determined by measuring the rate of decay of the vibrational state populations in the center of the reactor tube. At a pressure of 17 Torr and a temperature of 390 K, the V-V exchange rate is about 2×10^4/s which is roughly one tenth the rate molecules in the probe volume visit

the surface and about 10^3 times the wall deactivation rate. There is, therefore, significant probability that molecules deactivated at the wall will be re-excited by the V-V process before returning to the axis where the measurements are made. Thus, except for very small deactivation probabilities, the observed rates of decay of the populations versus residence time (i.e., the length of the specimen tube exposed to the gas divided by the flow velocity) will be slower than the actual wall rates. There are several likely mechanisms for direct energy exchange with the surface, each possibly at a different rate. Some mechanisms result from an event sequence referred to as a channel wherein there may be interactions between channels. There have been numerous discussions of the chemistry and thermodynamics on surfaces.[24, 25, 26, 27, 28, 29, 30] The measurements reported here were incapable of distinguishing among these mechanisms, but rather they provided an integrated evaluation of all active surface loss and gain mechanisms. Nevertheless, the accuracy of the measurements of these net loss rates was not diminished by this fact.

Molecules are reflected from the wall without loss of vibrational energy with a probability of $1 - \gamma_v$. With diffusion, as γ_v increases, a radial density profile in the vibrational level populations develops. In the experiments, the length-to-diameter ratio of the reactor tube was about 8, which, with the modest gas flow rates used, maintained a flat, "plug-type" radial velocity profile along the axis of the tube. The relationship between wall loss rate $k_{v(wall)}$ and probability γ_v is influenced by the cylindrical geometry of the reactor tube. Because the rate constant $k_{v(wall)}$ could be quite high, especially for v = 4 and 5, the following development retains all corrections. (Note that the "v(wall)" label is dropped temporarily.) The total flux of particles (particles per unit area per unit time) near a surface, J, is given by[31]

$$J = [N_2] \int_0^\infty f(v_r) v_r \, dv_r \qquad (9)$$

where $[N_2]$ is the number density of molecules, v_r, is the velocity normal to the wall (i.e.,in the radial direction) and $f(v_r)$ is the probability density of velocity. Assuming the Maxwell-Boltzmann velocity distribution function, the flux becomes

$$J = [N_2]\sqrt{\frac{k_B T}{2\pi m}} = \frac{1}{4}[N_2]\bar{c} \qquad (10)$$

where k_B is Boltzmann's constant, T is the absolute temperature, and $\bar{c}$ is the mean molecular speed. This expression must be modified when there are reflection and loss fluxes at the surface. The expression now is given in two equations which describe the transport to and from the wall.[32,33] Thus,

$$J_i^{\pm} = \frac{1}{2}[N_2]_i\left(\frac{1}{2}\bar{c}_i \pm w_0\right) \mp \frac{1}{2}D\nabla[N_2]_i \qquad (11)$$

for vibrational species i, where the flux toward the wall is J^+, J^- is the flux in the opposing direction, D is the coefficient of diffusion and w_0 is mean transport drift (flow) velocity towards the surface. Since the flow is only along the tube axis, $w_0 = 0$. Accounting for the loss at the surface, we have for that boundary condition

$$J_{@wall} = (1-\gamma)J_i^+ - J_i^- = 0 \qquad (12)$$

Substituting Eqs. (11) in to Eq. (12) and simplifying gives

$$-D\frac{\partial[N_2]}{\partial r} = \frac{\gamma[N_2]\bar{c}}{4\left(1-\frac{\gamma}{2}\right)} = \gamma J^+ \qquad (13)$$

Equation (13) shows that for $\gamma = 0$ the flux reduces to that given by Eq. (10). In situations where γ is small, the $(1 - \gamma/2)^{-1}$ in Eq. (13) can be neglected, but this is not generally applicable for the measurements reported here. The steady state diffusion equation can be written[34]

$$u_0 \frac{\partial [N_2]}{\partial z} = D \nabla^2 [N_2] \qquad (14)$$

where u_0 is the axial transport velocity. A solution of the form $[N_2](r, z) = [N_2](0,0)R(r)Z(z)$ is assumed, where (r,z) are, respectively, the radial and axial coordinates and there is no azimuthal dependence. Equation (14) can then be written in the form showing two equations for R and Z, namely

$$-\frac{u_0}{Z}\frac{\partial Z}{\partial z} + \frac{D}{Z}\frac{\partial^2 Z}{\partial z^2} = -\frac{D}{R}\frac{\partial^2 R}{\partial r^2} - \frac{D}{rR}\frac{\partial R}{\partial r} \qquad (15)$$

Since the two equations are independent, they must be equal to a common constant k_v, where the notation for the species in level v is reinstated. Thus, we have

$$\begin{aligned} \frac{\partial^2 Z}{\partial z^2} - \frac{u_0}{D}\frac{\partial Z}{\partial z} - \frac{k_v}{D}Z &= 0 \\ \frac{\partial^2 R}{\partial r^2} + \frac{1}{r}\frac{\partial R}{\partial r} + \frac{k_v}{D}R &= 0 \end{aligned} \qquad (16)$$

The appropriate solutions to the Eqs. (16) are $Z(z) = exp(k_{zv}z)$ and $R(r) = J_0(F_v\, r/r_0)$, where J_0 is the zero order Bessel function of the first kind and $F_v = r_0\,(k_v/D)^{0.5}$. Note that k_{zv} and k_v are wall rates in this development. Substituting the solution into the Z equation and solving for k_{zv} gives

$$k_{zv} = \frac{u_0}{2D} - \frac{u_0}{2D}\sqrt{1 + \frac{k_v}{D}\left(\frac{2D}{u_0}\right)^2} \qquad (17)$$

In the limit of $k_v << u_0^2/4D$, Eq. (17) reduces to $k_{zv} = -k_v/u_0$. Typically, this condition was satisfied to better than two orders of magnitude. The axial function now becomes

$$Z(z) = \exp(-k_v z/u_0) = \exp(-k_v t) \qquad \textbf{(18)}$$

where $t = z/u_0$ is the residence time of the gas in contact with the specimen wall. Equation (18) describes the exponential decay of the vibrationally-excited nitrogen gas along the specimen tube axis due to deactivation at the wall. Substituting the solution for the R equation into Eq. (13), gives at the wall with $r = r_0$, the expression

$$D\frac{F_v}{r_0}J_1(F_v) = J_0(F_v)\frac{\gamma_v \bar{c}}{4\left(1 - \frac{\gamma_v}{2}\right)} \qquad \textbf{(19)}$$

where J_1 is the first order Bessel function of the first kind. If the deactivation probability γ_v is known, then Eq. (19) is transcendental in wall rate k_v (i.e., $k_{v(wall)}$). However, since the rate was measured directly in this work, Eq. (19) can be solved for γ_v giving

$$\gamma_v = \frac{4DF_vJ_1(F_v)}{\bar{c}r_0J_0(F_v) + 2DF_vJ_1(F_v)} \approx \frac{4DF_vJ_1(F_v)}{\bar{c}r_0J_0(F_v)} \qquad \textbf{(20)}$$

In the limit of small γ_v, Eq. (20) reduces to $\gamma_v = 2r_0k_{v(wall)}/\bar{c}$. For example, for typical conditions used in this work, for a value of $k_{v(wall)} = 15.5\ s^{-1}$, this approximation is 8% smaller than the value of $\gamma_v = 5.07\times10^{-4}$ given by Eq. (20).

Master Equation Model

In order to determine the impact of the homogeneous contributions to the observed decay rates, a well-tempered theoretical treatment of vibrational energy exchange was explored. Homogeneous interactions, specifically the V-V processes, mask the interactions with the wall. The heterogeneous wall loss rates $k_{v(wall)}$ determined in these experiments were greater than V-T rates by about three orders of magnitude while the V-V rates were greater

than the wall rates by a similar amount. It is commonly assumed that $k_{v(wall)}$ increases linearly with v. Yet, there was some evidence early on in this work for deviation from a linear relationship to a function that peaks for $v \geq 4$. Moreover, for our conditions, the V-V "pumping" process is very efficient in creating a nonBoltzmann vibrational population distribution in the source gas that is subsequently altered by the interaction with the wall. These issues indicate that there will be a difference between the observed decay of the vibrational populations (i.e., the apparent wall rate) and the actual wall rate. Clearly, as shown in Eq.(20), the deactivation probability, γ_v, is not linearly related to $k_{v(wall)}$ due to the diffusion process. Since the CARS probe is located in the gas many mean free paths from the surface, it can be expected also that γ_v will not be linearly related to the observed decay rate. For these reasons, a concerted effort was made to fit simulations of the decay of vibrational populations in a cylindrical tube based on the Master Equation Model to all deactivation data in order to account for the impact of homogeneous interactions and diffusion.

The simulation code was previously written to predict the vibrational population distribution of nitrogen under only the influence of loss terms from homogeneous and heterogeneous vibrational modes.[2] The code development followed previous work of Bailey[35] and Capitelli.[36] Vibrational energy exchange influences certain chemical reactions in plasmas and flames. In diatomic molecules, this reactivity increases rapidly with v. Theory[37] and experiment[38] show the dissociative attachment threshold in hydrogen increases by five orders of magnitude from $v = 0$ to $v = 6$. The dissociation of 1% silane in active nitrogen was measured to be a factor of 70 larger than expected from theory.[39] Thus, a complete picture of the dynamics of our system requires more detailed knowledge of vibrational pumping and relaxation processes. The V-V exchange rates at high v's are particularly difficult to measure because the rates and molecular densities are extremely small. The V-V rates in the lower v's are better known and are extrapolated to high v's in the simulation code by the well known Schwartz, Slawsky and Herzfeld (SSH) theory.[40]

The V-V exchange rates are known to be much greater than the V-T rates at small v. The V-T rate increases rapidly with v and surpasses V-V around v = 28 depending on the translational temperature. It is unlikely that the V-T interactions had any direct influence on

the population distributions observed in this work, but they were included in the code to handle the upper population inversion extending to $v = 47$. The V-T process very rapidly removes population for $v > 47$. Translational temperatures in the measurements were always less than 400 K. These temperatures were determined by recording a rotationally-resolved CARS spectrum for the ground state band ($v = 0$ to v = 1) during each experiment and fitting a theoretical CARS spectrum to the measured spectrum. The theoretical spectrum was generated by the Sandia CARS code.[41] Rotational populations were observed to be Boltzmann distributed in all vibrational bands, and thus were equilibrated to the translational temperature. It was found that the rotational temperature was independent of v consistent with the results of Massabieaux et al.[42] It was assumed that this held in all experiments carried out in this work. With the modest temperature and low pressure used in these studies, three body collisions rarely occur. Because the gas temperature was somewhat less than 1000 K, the probabilities for multi-quantum V-V and V-T exchanges were very small compared to single quantum steps, and thus could be neglected.[43] All heterogeneous interactions also were calculated on a single quantum loss rate basis. The model assumed the molecule to be a Morse-type rigid oscillator. These concepts and limitations were applied to the Master Equation, which can be written in the generalized form

$$\dot{P}_i = \sum_k (\Gamma_{k,i} P_k - \Gamma_{i,k} P_i) \qquad (21)$$

here $\Gamma_{m,n}$ is the conditional probability rate of the transition m to n and P_n is the occupational probability of the property in question.[44] Here the property is the nitrogen number density, where each vibrational level is taken as a separate species. The expression used in the model is written[2]

$$\frac{dN_v}{dt} = N_{v+1} R_{v+1,v} + N_{v-1} R_{v-1,v} - N_v \left(R_{v,v+1} + R_{v,v-1} + k_{v(wall)} \right) \qquad (22)$$

where N_i is the number density (cm^{-3}) of a neutral nitrogen molecule in the i^{th} vibrational state of the ground electronic state, the $R_{i,j}$'s are the exchange rates (s^{-1}) containing the V-T and the V-V interactions and $k_{v(wall)}$ is the wall deactivation rate of the v^{th} vibrational state. The rates in the first two terms on the right side of Eq. (22) can be expanded in forms given by

$$R_{v+1,v} = P_{v+1,v}N + \sum_{k=0}^{v-1} Q_{v+1,v}^{k,k+1} N_k$$
$$R_{v-1,v} = P_{v-1,v}N + \sum_{k=1}^{v} Q_{v-1,v}^{k,k-1} N_k \qquad \textbf{(23)}$$

which represent the V-V and V-T rates of single quanta energy exchange between molecules wherein population is introduced into level v. For the V-V process, population increase of the v level given in the second term of the first expression in Eq. (23) derives from one level above by transferring energy to a second molecule and the corresponding term in the second expression describes the population increase from one level below by transfer of energy from a second molecule, where the $Q_{m,n}^{p,q}$, are the rate coefficients (cm^3/s). The first terms on the right sides of the two expressions in Eq.(23) correspond to V-T processes which increase the population of the v level, where the $P_{m,n}$ are the rate coefficients (cm^3/s) and N is the total number density of the gas. The corresponding loss rates given by the third and fourth terms of Eq.(22) have terms analogous to Eq.(23).

ANALYSIS

Data Collection, Corrections and Normalization

Plots of typical spectra for the v = 0, 1, 2 and 3 bands are shown in Fig. 3 The measurements were made at the peaks of the J = 8 lines of the vibrational bands. This simplified both the deactivation analyses and the saturation corrections; however, because of the narrow width of the rotational lines, the CARS signals were extremely sensitive to the wavelength setting of the dye laser. Since the YAG laser was operating single mode (0.006 cm^{-1}), the observed width was the convolution of the Doppler lineshape of the rotational line with the lineshape of the dye laser. Since the Doppler width was 0.006 cm^{-1} and the dye laser linewidth was about 0.1 cm^{-1}, the observed width was determined by the dye laser. The dye laser wavelength step size was 0.0005 nm (0.0135 cm^{-1}); however, the resetability was two to four times larger than this step size. Thus, it was very difficult to dependably move from one vibrational band to the next without misalignment of the dye laser wavelength. Therefore, the rotational line in each vibrational bands was scanned and then fitted to the squared Lorentzian function. This procedure provided a precise measurement of the peak CARS intensity with a much relaxed requirement for the initial wavelength setting of the dye laser. This type spectral measurement is termed "skip spectra."

Skip spectra were obtained in both deactivation and saturation experiments. In a typical experiment, which involves several runs over the desired vibrational bands, each J = 8 line is scanned with 16 spectral points. At each spectral point in a scan, the average of 200 to 500 laser pulses was recorded. For each laser pulse, the PMT produces a signal CARS pulse that is integrated with 10-bit precision by the LeCroy ADC. The signals from the two laser-monitoring PIN diodes are also integrated with the ADC and, with the integrated CARS signals, are averaged at each spectral point. Signal data are recorded in double precision for each spectral point and stored in files as sums. This includes the sum and the sum of squares for the CARS, dye and YAG PIN diode signal as well as the wavelength and number of pulses summed. For the laser covariance, the sums of sums and sums of differences of diode signals

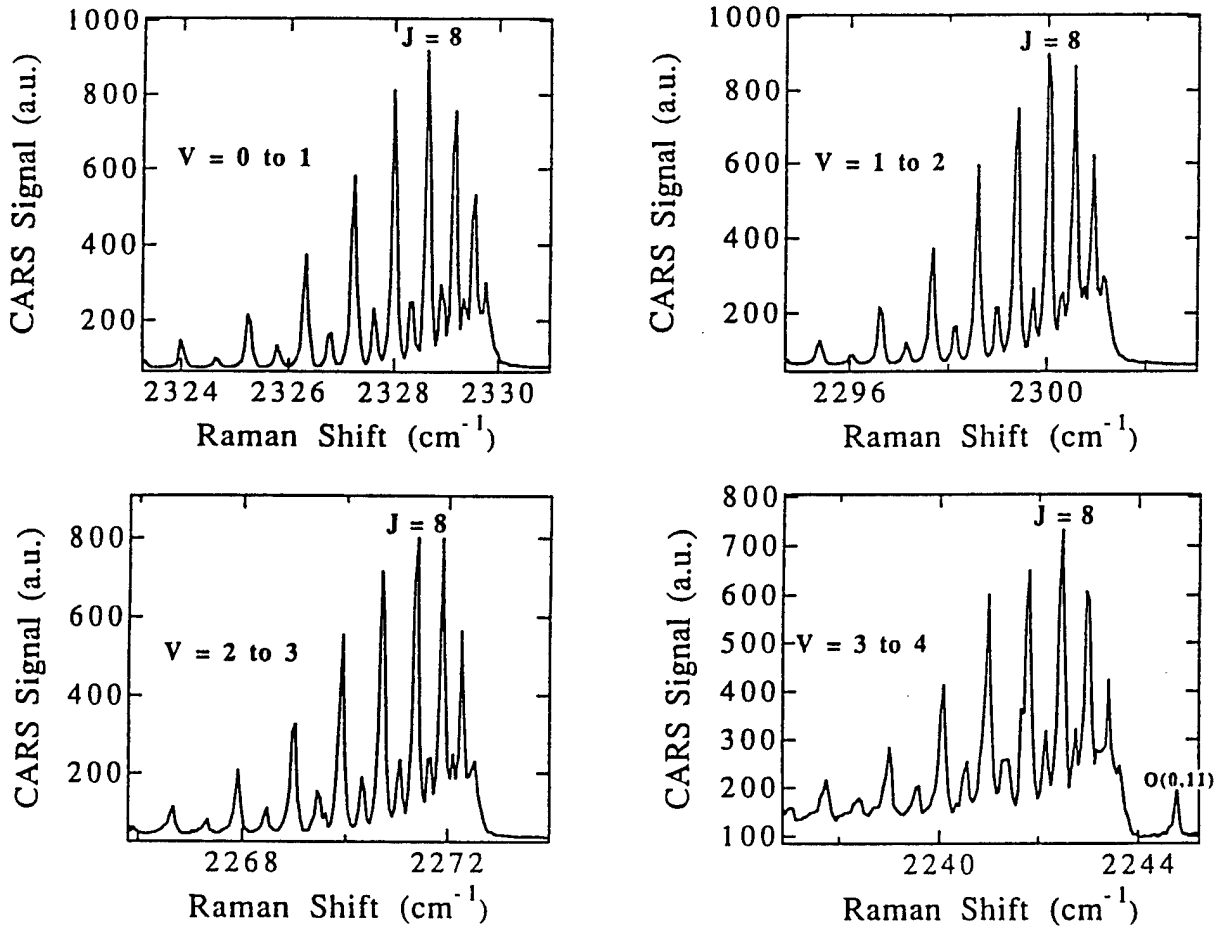

Figure 3. Plots of the v = 0, 1, 2 and 3 rotational-vibrational Q branch bands of N_2 obtained with the CARS system in Fig. 2.

and their sum of squares are also written to the file. Separately, hand records were kept of the optical attenuation of the CARS beam, electronic channel gains and the beam powers between each run. The files and notes were used to determine the rescaled spectral value, saturation correction and the statistics.

Rescaling of data differs between a saturation and a deactivation experiment. For the saturation case, each band v is normalized separately to known YAG and dye laser powers. In the deactivation case, an entire run is rescaled using the average PIN diode signals from the v = 0 measurements as the reference values and then the raw CARS signals are corrected for saturation. The rescaling places the measurements on each vibrational band in a given deactivation experiment on the same the basis of YAG and dye powers so that the relative band populations can be extracted. Examples of these calculations are

$$S_{ci} = \sum_{j=1}^{npts} sig_{i,j} \qquad S2_{ci} = \sum_{j=1}^{npts} sig_{i,j}^2$$
$$Y_i = \sum_{j=1}^{npts} yag_{i,j} \qquad D_i = \sum_{j=1}^{npts} dye_{i,j} \qquad \textbf{(24)}$$

where the sums are for each spectral point i of the band v, $S_{c,i}$ is the CARS signal sum, $S2_{c,i}$ is the sum of the squares of the CARS signals, Y_i is the sum of the yag PIN diode signals, and D_i is the sum of the dye PIN diode signals. The lower case quantities are the pulse values and the means over npts pulses are calculated later.

Each rotational line was scanned with np points that includes two points in the background. The CARS background signals were measured close to the band heads of each vibrational band in regions essentially free of any detectable rotational lines. The background measurement is subtracted from the average signals, which removes any electronic offset and nonresonant CARS signal. The CARS channel offset came from two external sources. One was a slight sensitivity to extraneous electrical emissions, principally from the flash lamp power supply, and the other was leakage of the 532 nm light onto the PMT. Electronic offsets in PIN diode channels did not change more than five counts in three years and was,

thus constant throughout an experiment. Offsets in the PIN diode channels, D_{off} and Y_{off}, were determined by observing the dark count value for each detector, which was typically 25 counts.

CARS background exhibited a slight gradual change across a vibrational band. This characteristic was constant through an experiment and probably over many experiments. Actually, the nonresonant background was weak or nonexistent. A conventional background correction uses measurements on either side of the feature to predict the background at the peak of the line. In this work, the value on one side was subtracted, which provided a consistent and expedient method. The error was usually well under 10 counts or 1%. This error was largest in the high hot bands where the signal-to-background ratio was the lowest.

The band averages for the dye laser and YAG laser PIN diode signals over np spectral points are computed from

$$D_v = \left[\frac{1}{np}\sum_{i=1}^{np}\frac{D_i}{npts}\right]_v - D_{off} \quad , \quad Y_v = \left[\frac{1}{np}\sum_{i=1}^{np}\frac{Y_i}{npts}\right]_v - Y_{off} \tag{25}$$

where D_{off} and Y_{off} were 25, and the rescaled CARS signal, S_{c2i}, was calculated for each spectral point i in band v as given in by

$$S_{c2i} = (S_{ci} - S_{off})\left(\frac{D_v}{D_i - D_{off}}\right)\left(\frac{Y_v}{Y_i - Y_{off}}\right)^2 \tag{26}$$

which normalizes each spectral datum to the YAG and dye power averages for that scan. The variances of the means of the CARS signals, the dye and YAG PIN diode signals and the covariance between the dye and the YAG diode signals were also calculated. The correlation coefficient between diode signals was typically between 0.2 and 0.1 or less which supports the normalization using the averages.

Saturation corrections, derived from calibration experiments,[15] were used to correct the reduction in response caused by stimulated Raman scattering (SRS) which pumps

population directly into the upper level simultaneously with the CARS process.[15, 45] Saturation calibration measurements, which gave the relationship between the peak CARS signals and laser powers, would be conducted typically within no more than 20 days of the deactivation experiments to which the calibration was applied providing that the optical alignment of the system had not been disturbed. The average dye laser power was varied in steps from ~33 to ~10 mW for the saturation measurements. Usually, 30 mW (1.5 mJ/pulse at 20 Hz) was the power used in the deactivation experiments. Power incident on the main chamber was a convenient unit for the calibration of two PIN diodes. The J = 8 line was scanned in at least three of the normally detected hot bands of v = 1, 2, 3, and 4 at each dye laser power step while holding all other system variables constant. Nine to 12 power steps were recorded. Using the procedure described by Yaney and Parish,[15] the average CARS signal (PMT counts) in band v, S_{c2v}, at the J = 8 peak and the laser powers Y_v and D_v (PIN diode counts) were combined to plot $(S_{c2v}/D_v \cdot Y_v^2)^{0.5}$ versus $D_v \cdot Y_v$ for each v-band. Parameterized in this way, the data gives a linear relationship for each vibrational band with an intercept b_v at zero laser power and a slope m_v as given in

$$\sqrt{\frac{S_{c2v}}{D_v Y_v^2}} = b_v + m_v D_v Y_v \qquad \textbf{(27)}$$

where m_v is negative. The square root of the ratio of the unsaturated to saturated signal, S_{satv}, gives the correction factor for each vibrational level as[15]

$$S_{sat\,v} = \frac{1}{1 + \frac{m_v}{b_v} D_v Y_v}. \qquad \textbf{(28)}$$

The ratio m_v/b_v in Eq.(28) generally is a linear function of v.[15] Therefore, doing a linear regression of these ratios to v + 1 from as few as three v bands provided a convenient way to accomplish the correction of the deactivation data for all v bands under each particular set of experimental circumstances. Since the PIN diode responses to the powers of their respective lasers had been calibrated, the saturation calibrations could be used to correct the

deactivation data using count values in Eq.(28). It can be shown that the methods used are equivalent to using power values. The deactivation and saturation experiments were connected by diode counts-per-mW (cnts/mW) ratios which were used to convert deactivation power readings to appropriate saturation values.

The saturation measurements were normally carried out by varying the dye laser power by rotating a halfwave plate just in front of a polarizer while holding the YAG power constant. To check that the saturation effect depended on the product of the two laser intensities in the probe volume as shown in Eq.(28), the YAG power was varied in one experiment while holding the dye power constant. The CARS signal had the same saturation dependence on the incident YAG power as it did by varying the dye power.

The data at the spectral points, S_{c2i}, are free of offset, background and any laser power drift during the scan over the line. These spectral data of the rotational lines were fitted to a Lorentzian squared function to obtain the peak heights as discussed in the next section. The rotational peak heights were then corrected for saturation and the resulting values were rescaled to the average YAG and dye laser powers present during the measurements on the v = 0 to 1 ground-state band in that experiment. However, the optical attenuation and the amplifier gain were adjusted for each hot band to fit the observed signals well within the 1024-count digitization range of the ADC. The dynamic range of signals over the four or five vibrational bands was greater than 7×10^5. This dynamic range was covered by the neutral density filter wheel that provides attenuations from unity to 2145 and the amplifier that has 10 gain steps from unity to 10. Generally, the attenuation and the gain were adjusted to keep the maximum CARS signal pulses within 750 counts or less of the ADC. The CARS signals displayed considerable fluctuations attributed to the mode beating in the dye laser pulse which made these adjustments very critical to acquiring viable data.

Fitting the rotational line

In order to achieve a high degree of precision in determining the CARS signal strength, the J = 8 rotational line in each vibrational band was measured by scanning this line using, typically, 14 steps of 0.0005 nm (0.0135 cm^{-1}) and 200 laser pulses per step plus two background steps. The background signal level was removed from these raw data and the

square of the Lorentzian profile was used to fit to the background-free data using nonlinear regression analysis. This profile can be written for narrow lines in wavelength form as

$$L(\lambda_i) = \left\{ \frac{w_1}{1 + [(w_2 - \lambda_i)/w_3]^2} \right\}^2 \qquad (29)$$

where w_1 is the square root of the peak CARS amplitude of the line, w_2 is the wavelength at the peak, w_3 is the linewidth (FWHM) and λ_i is the wavelength at the i^{th} point of the scan. Because any background signal was removed prior to applying Eq. (29), no additive constant was needed in the expression. Parameter w_1 is proportional to the population difference $N(v, J = 8) - N(v + 1, J = 8)$, which was then used to compute the relative populations among the observed vibrational bands. The fitted values for w_1 were recorded in a disk file together with the PIN diode count averages, D_v and Y_v. These values of w_1 were then fully corrected, as stated at the end of the last section, to the ground state laser powers and for saturation. The corrected values, w_{gv}, for band v are obtained from

$$w_{gv} = w_{1v} S_{sat\,v} \frac{Y_0}{Y_v} \sqrt{\frac{A}{G} \frac{D_0}{D_v}} \qquad (30)$$

where Y_0 and D_0 correspond to the average ground state (v = 0 to v = 1) laser power values, G is the amplifier gain and A is the optical attenuation used in the band v measurements.

Obtaining the observed deactivation rates

Following the various normalizations and corrections of the peak values of the J = 8 line in each vibrational band, the data for the v bands at each residence time were processed together to extract fractional populations. The residence time is simply the length of the specimen tube exposed to the vibrationally-excited gas divided by the gas flow velocity in the tube. It is important to emphasize that the peak line strengths, w_{gv}, obtained at a given residence time were processed together independent of the data at other residence times. As

shown in Eq.(8), the line strength is proportional to the CARS susceptibility, χ_{CARS}, which is given by[18]

$$\chi_{CARS} = \frac{8\pi^2 n_p \epsilon_0 c^4}{n_s \hbar \omega_s^4 \left(\omega_{ab} - \omega_p + \omega_s - i\frac{\Gamma_{ab}}{2} \right)} (N_a - N_b) \frac{\partial \sigma}{\partial \Omega} \qquad (31)$$

where the frequency ω_{ab} is the frequency of the transition between levels a and b, $\partial\sigma/\partial\Omega$ is the differential cross section of the linear Raman process which depends on v, *p* and *s* identify pump and probe (Stokes) quantities, $\hbar$ is Planck's constant divided by 2π, N_a and N_b are the population densities and Γ_{ab} is the line width. The total susceptibility includes the real and imaginary parts obtained from Eq.(31) and a nonresonant component as shown in Eq.(32).

$$\chi_{tot} = \chi_{CARS} + i\chi_{CARS} + \chi_{nr} \qquad (32)$$

If the nonresonant component has sufficient magnitude it can complicate the functional form of the CARS spectrum due to the squaring in Eq.(8). In this work, χ_{nr} was essentially zero. At resonance when $\omega_p - \omega_s = \omega_{ab}$, which corresponds to the peak of the line, only the imaginary part of Eq.(31) remains. Thus, using the peak line strength simplifies the analysis. It is assumed in this analysis that the rotational temperature, and therefore the rotational population distribution, is equilibrated with the translational or gas temperature. The population distribution over v and J is adequately described by

$$N_{v,J} = \frac{N}{Z} \exp\left[-\frac{G(v)}{kT_v}\right] g_J (2J+1) \exp\left[-\frac{B_e J(J+1)}{kT_r}\right] \exp\left[\frac{\alpha_e (v+\frac{1}{2}) J(J+1)}{kT_r}\right] \qquad (33)$$

where N is the total density of molecular nitrogen, Z is the partition function, G(v) is the vibrational term energy from the ground state, v and J are, respectively, the vibrational and rotational quantum numbers, B_e is the equilibrium rotational constant, α_e is the vibration-

rotation interaction constant, T_v is the vibrational temperature of band v corresponding to the v to v + 1 transition, T_r is the rotational temperature, k is the Boltzmann constant and g_I is the statistical weight due to nuclear spin degeneracy which depends on J for nonzero nuclear spin. The partition function is found by summing Eq.(33) over v and J; however, it can be factored into vibrational and rotational parts with, at most, a 1% error by neglecting the right hand factor involving v and J in Eq.(33). Thus,

$$\begin{aligned} Z &= Z_v Z_r \quad where \; Z_v = \sum_v \exp\left[-\frac{G(v)}{kT_v}\right] \\ and \quad N_v &= \frac{N}{Z_v}\exp\left[-\frac{G(v)}{kT_v}\right] \end{aligned} \tag{34}$$

and Z_r is the sum of the J-only-dependent factors in Eq.(33). The population difference for a Q Branch transition where $\Delta J = 0$, $\Delta N_{v,J} = N_{v,J} - N_{v+1,J}$ can be written as

$$\begin{aligned} \Delta N_{v,J} &= K'_J (N_v K_{v,J} - N_{v+1} K_{v+1,J}) \\ where \quad K_{v,J} &= \exp[\alpha_e (v+0.5) J(J+1)/kT_r] \\ and \quad K'_J &= g_I (2J+1)\exp[-B_e J(J+1)/kT_r]/Z_r \end{aligned} \tag{35}$$

From Eqs.(8) and (33), the square root of the CARS signal can be written

$$\begin{aligned} S_{v,J} &\propto I_p I_s^{0.5} \Delta N_{v,J} \sigma_v \\ and \; \sigma_v &= \sigma_0 (v+1) h(v) \end{aligned} \tag{36}$$

where σ_v is the Raman cross section of the v vibrational band and h(v) corrects for the deviation of the Morse potential from an harmonic oscillator.[46] The width of the Doppler-broadened rotational-vibrational line depends on the frequency of the transition and the gas temperature. This introduces another correction factor, D_v, given by[46]

$$D_v = \sqrt{\frac{\omega_{v,J}}{\omega_{0,J}}}, \quad where \quad \omega_{v,J} = E_{v+1,J} - E_{v,J} \tag{37}$$

The strength of the transition is inversely proportional to the width. $E_{v,J}$ is the energy of the rotational-vibrational level and Eq.(37) references the strength of a transition in band v to the ground state band v = 0. All measurements were made on J = 8. Combining Eqs.(35)-(37) assuming constant laser powers, perfect phase matching and constant beam intersection geometry, the square root of the CARS signal becomes

$$S_{v,J} = C_J (v+1)\, h_v D_v (K_{v,J} N_v - K_{v+1,J} N_{v+1}) \qquad \textbf{(38)}$$

where C_J contains the laser power factors and all the constants in Eqs. (8), (31), and (34)-(36). At some v band the population will be so small that the signal will be unmeasurable. It is assumed that populations at higher v's had negligible affect on the measured populations in the lower v bands. This permitted a truncation of the calculation for extraction of fractional populations. Thus, by solving Eq.(38) for N_v gives a summation from v to the maximum v measured, v_{max}, which for J = 8, yields Eq.(39), where $N_v' = N_v C_J$ is a relative population.

$$N'_v = \frac{1}{K_{v,8}} \sum_{v'=v}^{v_{max}} \frac{S_{v',8}}{(v'+1)\, h_{v'} D_{v'}} \qquad \textbf{(39)}$$

In this summation, the population of the v_{max} +1 band is set to zero. The total relative population, N', is then the sum of Eq.(39) from v = 0 to v = v_{max}. Thus, the fractional populations, F_v, are found from

$$F_v = \frac{N'_v}{\sum_{v=0}^{v_{max}} N'_v} = \frac{N_v}{\sum_{v=0}^{v_{max}} N_v} \qquad \textbf{(40)}$$

Various schemes were explored to extrapolate the calculation of F_v to include higher values of v_{max} based on theoretical projections. Although these extrapolations produced small changes in the values of F_4 and F_5 compared to the above truncation procedure, these changes had, at most, only a small impact (<10%) on the observed deactivation rates.

DATA AND RESULTS

Tables 1-6 summarize the results of this project. Reproducibility of these results varied because of accumulated surface changes due to use of the specimen in many experiments, planned treatments of the specimens, undetermined variations in the specimens or uncontrollable variations in the experimental system. Several experiments with Pyrex tested these possibilities. Tables 1, 3 and 5 report the observed deactivation rates, $k_{v,}$, and Tables 2, 4 and 6 give the corresponding apparent deactivation coefficients, γ_{va}, computed directly from the k_v (viz., instead of $k_{v(wall)}$) values using Eq.(20). Generally, $k_{v(wall)}$ is expected to increase for higher pressure and decrease with increased temperature. For a given pressure, the temperature for specified discharge conditions was determined by the gas flow rate. Higher flow rates gave higher temperatures due to increased heat transport. The observed deactivation rate, however, is a combination of the interactions of the molecules with the wall and the interactions with other molecules through the V-V exchange process. This greatly complicates the interpretation of the data. The fitting of the Master Equation Model attempts to extract the wall deactivation rate, but the interplay between these two interactions can vary significantly from experiment to experiment. The results of these fittings are discussed in the next section.

Except for gold, all surfaces were found to be nitrided by the afterglow due to the small density of nitrogen atoms.[47] This density was estimated to be 0.55% of $[N_2]$ from measurements of the decay of the first positive emission, $B^3\Pi_g$ to $A^3\Sigma_u$, versus residence time. Surface measurements on Pyrex using XPS showed nitrogen bonded principally to the silicon and secondarily to the oxygen surface atoms of witness coupons.[48] The complete XPS results are reported in a later section. Coverage was determined to be between 8% and 10% of the surface with one case showing about 30%. It is clear that exposure to the afterglow changes the surface in some way. The details of the bonding mechanisms cannot be obtained nor completely understood from these experiments. Nitrogen adatoms are expected to make the surface passive by permanently occupying surface adsorption wells generated by dangling bonds. They also change the principal surface resonance vibration away from that of the

virgin surface which could provide more efficient coupling to vibrating molecules. Thus, adatoms may either increase or reduce the surface deactivation rate and, in the same respect, the number of surface collisions a molecule makes or the number of quanta lost per collision may be impacted by the nitriding.

Pyrex

Table 1 gives the observed values of k_v with fitting uncertainties and Table 2 gives the corresponding apparent deactivation coefficients γ_{va}. These tables also contain results of Master Equation modeling efforts. In Table 1, "nitrided" indicates the surface had been exposed to active nitrogen (i.e., afterglow) in several previous experiments and was found from XPS measurements to have nitrogen bonded to the surface; "neat" refers to the first time this specimen was used, taken as is from the glass shop and treated only to a general cleaning; "+column" refers to an experiment where the tube was placed in the positive column for 33.7 hours before the deactivation measurements; and "exposed" refers to an experiment where the tube spent 39.5 hours in the afterglow before deactivation measurements. The cleaning procedure generally consisted of ultrasonic degreasing in methylene chloride followed by ion cleaning at about 5 Torr in flowing argon for 30 to 60 minutes.

Experiments 1 and 2 used the same tube wherein the latter experiment occurred after additional exposure of the tube to the afterglow thereby increasing the degree of nitriding. It would seem that the additional nitriding in Experiment 2 is responsible for the higher values of γ_{va}. The lower flow rate and the resulting lower temperature introduces ambiguity in any attempt to interpret these data. Changes due to exposure to the afterglow were also reported by Black et al. using a microwave source[8]; however, they report a decrease of γ_1 for Pyrex after a 24 hour exposure to the afterglow. They found no change with exposure when using a thermal source. This can be explained by the fact that they measured only the v = 1 band using a 1-m long specimen tube. With the microwave source, as with the positive column source used in this work, the vibrational population is distributed across all low-v states corresponding to a vibrational temperature typically well above the 2000 K they report for their thermal source. Moreover, there is no surface nitriding using a thermal source. Thus, measuring only the v = 1 population produced by a discharge source is not sufficient to

correctly characterize the population changes due to wall deactivation over long residence times, especially with V-V pumping and nitriding effects.

Experiments 3 and 4 were carried out to check for reproducibility and the degree of dependence on pressure. The data and fitting results for Experiment 3 are given in Fig. 4. The flow rate in Experiment 4 was not increased to compensate for the higher pressure; therefore, the temperature in Experiment 4 was not the same as in Experiment 3. Nevertheless, the deactivation rates in these two experiments are the same within fitting uncertainties. Experiment 5 attempted to achieve a high degree of nitriding. Although the γ_{va} values are larger than the values obtained for the "neat" specimens, the rate of increase of γ_{va} with v for the "+ column" specimen is about half that of the neat specimens. Experiments 4, 6 and 7 used one tube and Experiment 7 followed the next day after Experiment 6. Experiments 6 and 7 were run to test reproducibility. The γ_{va} values show reasonable agreement within the fitting uncertainties plus the estimated 5 to 10% uncertainty in the repeatability of the set up of the experimental conditions. Comparison of Experiments 6 and 7 to Experiment 4 again shows the rate of increase of γ_{va} with v to be slower after the tube was exposed to the afterglow. An experiment was attempted at a pressure of 0.5 Torr also on the this specimen. Although the signals were very weak, the observed deactivation rates for v = 1 and 2 were about half the values obtained in Experiments 6 and 7 confirming the expected pressure dependence.

Gold Foil

The results reported in Tables 2 and 3 are for the same gold foil and are tabulated in order of acquisition. The foil was formed to completely cover the inside of a Pyrex tube. Gold was chosen because surface changes due to reaction with active nitrogen were not expected. Thus, experiments could be conducted to assess the effects of temperature (determined by the gas flow rate) and pressure in the absence of nitriding. It should be noted, however, that the surface did change from a calendered gloss to a slightly darker, very fine buff. This surface roughening could only be caused by collisions of vibrationally hot nitrogen during the experiments or by the argon positive column used for surface cleaning. The first three experiments in Tables 3 and 4 used three different gas flow rates in order to vary the gas

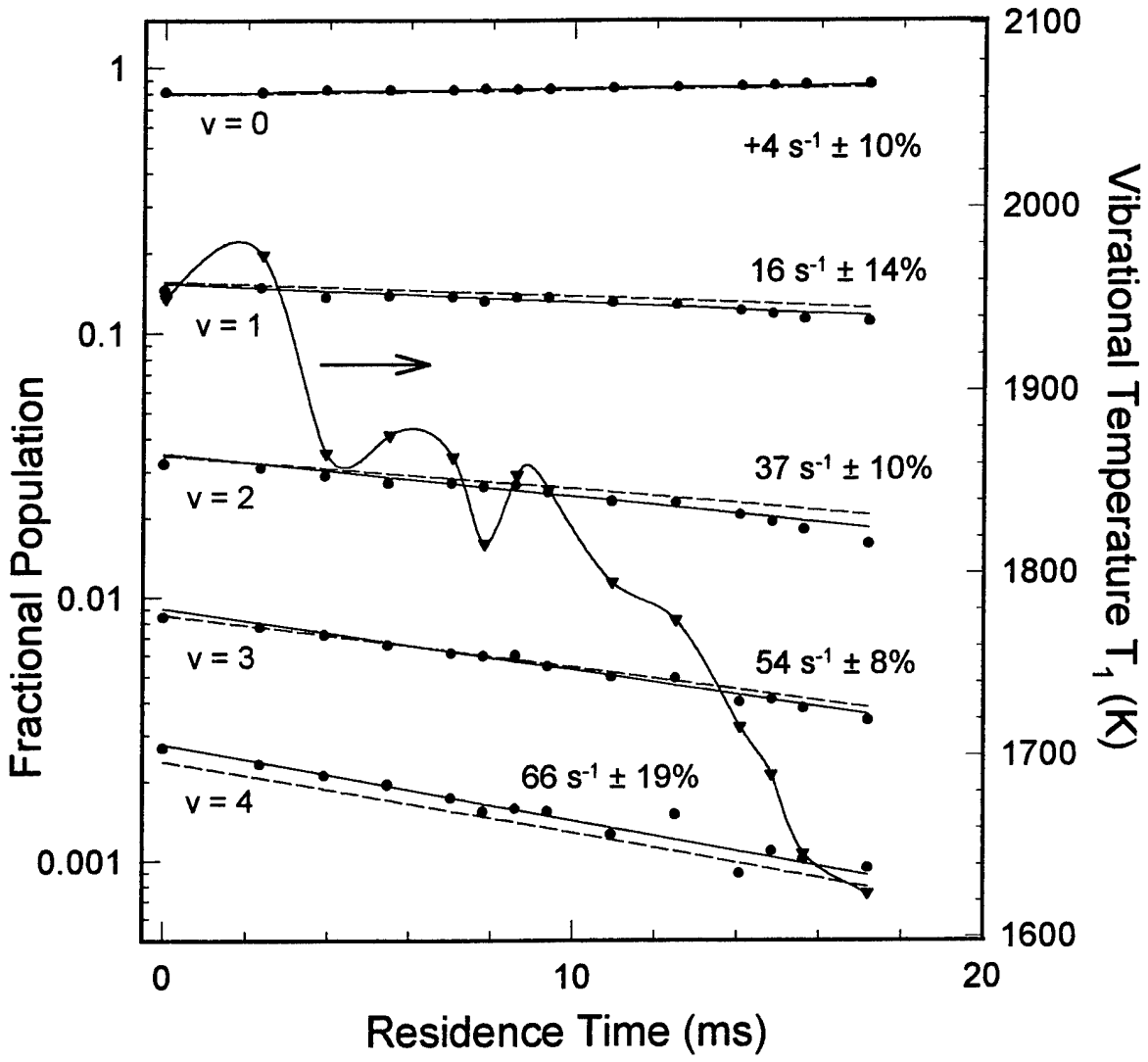

Figure 4. Deactivation measurements on neat Pyrex at 360 K and 11 Torr. The points are the data; the solid lines are expontential fits to the data with the rates given; the dashed lines are the results of the fitting of the Master Equation Model to the data; and the vibrational temperature of the v = 1 band, T_1, is given by the triangles joined by the cubic spline curve.

temperature. The tube was mounted in the chamber using glass beads that provided good thermal isolation. Thus, it is assumed that the tube temperature was equal to the gas temperature as measured from a CARS rotational spectrum. As expected, the deactivation rates decreased uniformly with increase in temperature. The last three experiments were intended for pressure studies. Comparing Experiments 1 and 4, which are at the same temperature, show significant decreases in deactivation rates and the corresponding γ_{va} values with drop in pressure; however, the opposite change is shown in Experiments 2 and 5 which were performed at a higher temperature. It is likely that this apparent contradiction is a consequence of the complexities of the mixing of the wall deactivation effects and the V-V interactions. The data and fitting results for Experiment 2 are given in Fig. 5.

Selected Materials

Tables 5 and 6 report the results on a variety of materials in the same form as the previous tables. The two stainless steel specimens showed the highest deactivation rates as would be expected and as reported by Black et al.[8] The 304 alloy was measured at the start of these studies when the discharge tube was operated at a higher temperature; however, the inside surface of this tube had been machined to a fairly rough surface. On the other hand, the AMS 312 tube had a very smooth "drawn" surface. Although the alloys are different, the high deactivation rates obtained with the 304 specimen is attributed to the large effective surface area. Figure 6 shows plots of the data and the fitting results for AMS 312. Two sets of values are given for aluminum which represent experiments on two different tubes of the same alloy. The results are in reasonable agreement which, again, shows that the measurement procedures were carried out in a consistent manner. The results for titanium were a surprise. The same tube was used in both experiments. Experiment 3 was first and showed virtually no deactivation of the v = 1 band while Experiment 4 showed that the surface had been altered by the exposure to active nitrogen. This nitriding again reduced the rate of increase of deactivation rate with v, which is a factor of two between Experiments 3 and 4. Titanium gave the lowest deactivation rates observed in these studies, which has to be attributed to the oxide layer on the titanium surface. Teflon, chosen to represent polymer-based materials, was expected to be benign. This material, indeed, gave the lowest deactivation rates

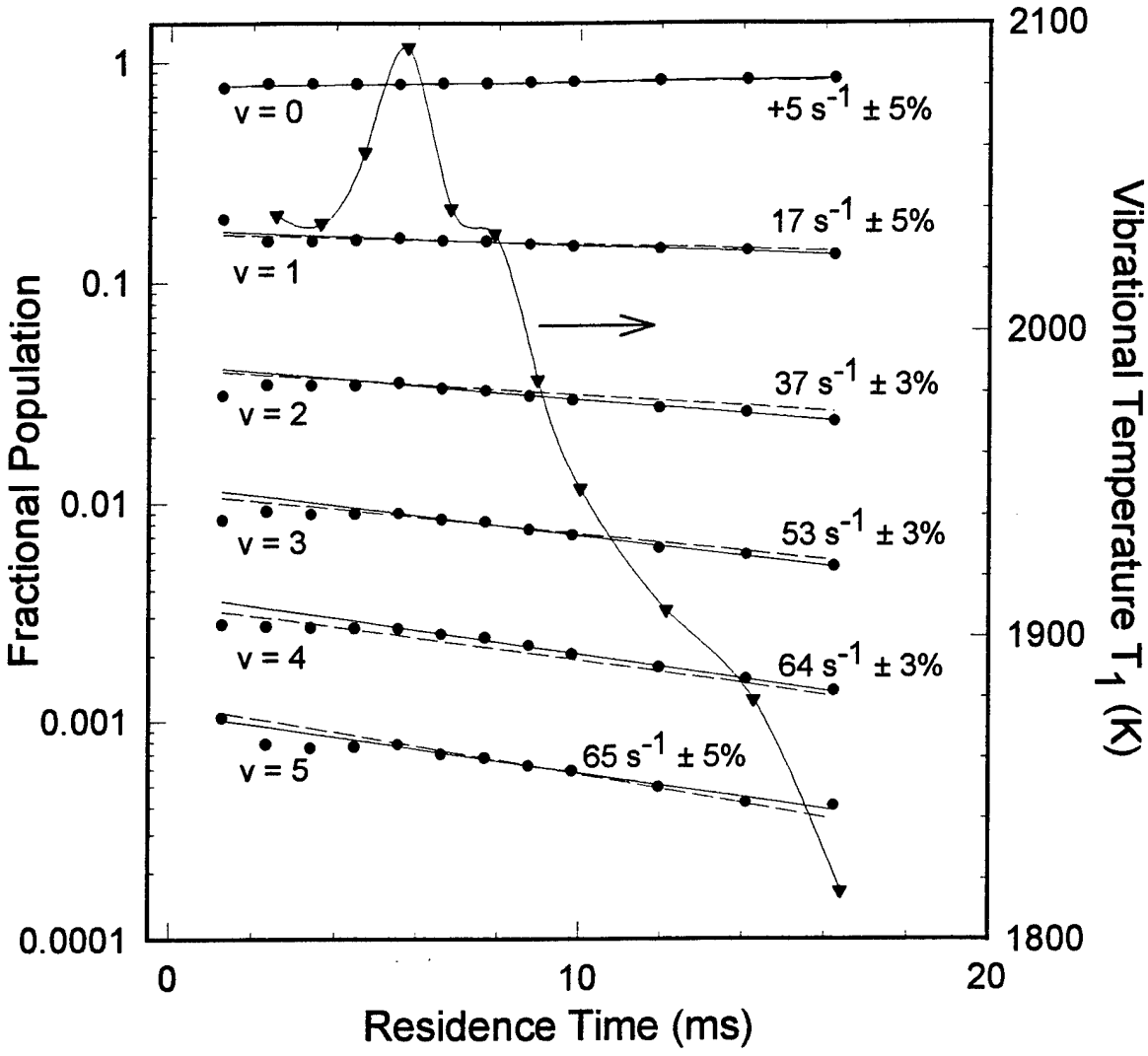

Figure 5. Deactivation measurements on gold foil at 351 K and 17 Torr. The points are the data; the solid lines are expontential fits to the data with the rates given; the dashed lines are the results of the fitting of the Master Equation Model to the data; and the vibrational temperature of the v = 1 band, T_1, is given by the triangles joined by the cubic spline curve.

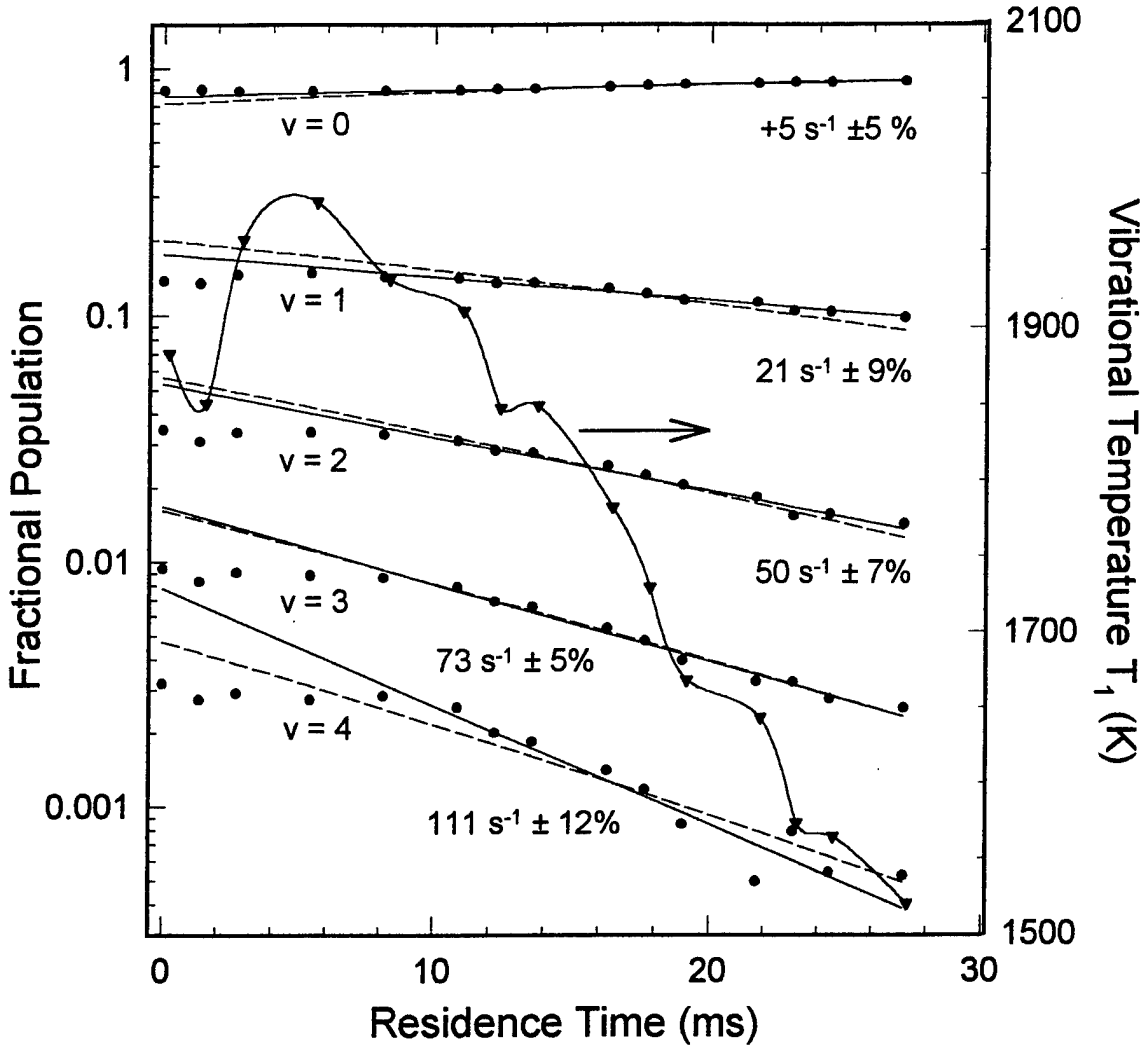

Figure 6. Deactivation measurements on AMS 312 stainless steel at 340 K and 14 Torr. The points are the data; the solid lines are exponential fits to the data with the rates given; the dashed lines are the results of the fitting of the Master Equation Model to the data; and the vibrational temperature of the v = 1 band, T_1, is given by the triangles joined by the cubic spline curve.

except for titanium. With two fluorine atoms per carbon atom, Teflon contains a high fluorine fraction which would otherwise contribute to strong deactivation. The stability of these bonds is generally quite high, and therefore Teflon would be expected to have only a weak interaction with vibrational-excited species. Nevertheless, it was found very important to keep the gas temperature low with this material, otherwise the surface would be altered and release contaminates into the flow.

Table 1: Observed deactivation rates k_v for Pyrex

Exp	Surface	T (K)	p (Torr)	Gas Flow (sccm)	k_1 (s^{-1})	k_2 (s^{-1})	k_3 (s^{-1})	k_4 (s^{-1})
1	nitrided	315	17	600	7.2 ±6%	20.2 ±4%	24 ±7%	26 ±10%
2	nitrided	307	17	450	12.9 ±3%	28 ±3%	37 ±7%	- - -
3	neat	360	11	802	12 ±14%	30 ±7%	47 ±5%	58 ±9%
4	neat	330	14	800	11 ±12%	31 ±5%	46 ±2%	62 ±5%
5	+column	321	11	800	19 ±11%	38 ±5%	57 ±5%	74 ±11%
6	exposed	325	14	800	14.9 ±5%	34 ±5%	47 ±4%	61 ±4%
7	exposed	328	14	800	14 ±7%	28 ±13%	42 ±7%	51 ±9%

Table 2. Apparent deactivation coefficients $\gamma_{va} \times 10^4$ for Pyrex[a]

Exp	γ_{1a}	γ_{2a}	γ_{3a}	γ_{4a}
1	2.4	7.6	9.5	10
2	4.6	11.8	18	- - -
3	2.7	9.7	17.4	21
4	3.5	11.9	19.7	32
5	6.7	17.2	28.3	35
6	5.1	13.6	21	32
7	4.7	11	18	24

[a] The %uncertainty in $\gamma_{va} \approx (1+0.01k_v) \times$%uncertainty in k_v

Table 3: Observed deactivation rates k_v of gold foil

Exp	T (K)	p (Torr)	Gas Flow (sccm)	k_1 (s^{-1})	k_2 (s^{-1})	k_3 (s^{-1})	k_4 (s^{-1})	k_5 (s^{-1})
1	323	17	600	22 ±4%	51 ±2%	62 ±3%	73 ±3%	---
2	351	17	900	17 ±5%	37 ±3%	53 ±3%	64 ±3%	65 ±5%
3	379	17	1200	7.5 ±9%	19 ±6%	32 ±4%	42 ±4%	50 ±4%
4	323	10	900	10 ±11%	20 ±4%	34 ±5%	42 ±8%	48 ±6%
5	353	23	900	15.7 ±6%	28 ±3%	48 ±6%	60 ±9%	---
6	340	14	800	20.7 ±4%	47 ±7%	67 ±4%	83 ±4%	---

Table 4. Apparent deactivation coefficients $\gamma_{va} \times 10^4$ of gold[a]

Exp	γ_{1a}	$\gamma_{2\alpha}$	γ_{3a}	γ_{4a}	$\gamma_{5\alpha}$
1	8.2	25.9	38	57	---
2	6.6	14.9	25	33	32
3	2.2	6.0	11.0	15.4	20
4	3.1	6.8	12.1	16	19
5	5.3	11.0	24	41	---
6	7.0	19	33	49	---

[a] The %uncertainty in $\gamma_{va} \approx (1+0.01k_v) \times$ %uncertainty in k_v

Table 5. Observed deactivation rates k_v of selected materials

Exp	Material	T (K)	p (Torr)	Gas Flow (sccm)	k_1 (s^{-1})	k_2 (s^{-1})	k_3 (s^{-1})	k_4 (s^{-1})
1	Stainless steel S 304	460	17	1000	53.1	108	138	- - -
2	Stainless steel AMS 312	340	14	800	19 ±9%	44 ±5%	70 ±6%	135 ±7%
3	Aluminum 3003	392 349	17 14	1000 800	12 8.3 ±7%	20 20 ±7%	31 32 ±6%	38 42 ±6%
4	Titanium AMS 4943D	382	14	1100	≈0	5 ±26%	8 ±21%	13 ±20%
5	Titanium AMS 4943D	375	14	800	1.3 ±22%	3.7 ±11%	6.4 ±9%	8.1 ±8%
6	Teflon	334	14	800	3.4 ±15%	8.8 ±10%	14 ±7%	20 ±8%

Table 6. Apparent deactivation coefficients $\gamma_{va} \times 10^4$ of selected materials[a]

Exp	Surface	γ_{1a}	γ_{2a}	γ_{3a}	γ_{4a}
1	SS 304	18	53	96	- - -
2	SS 312	7.8	23	58	10^4
3	Al 3003	4 2.8	7.0 7.3	12 12.7	15 18.3
4	Ti 4943D	≈0	1.5	2.5	4.3
5	Ti 4943D	0.4	1.2	2.1	2.9
6	Teflon	1.1	2.8	4.7	7

[a] The %uncertainty in $\gamma_{va} \approx (1+0.01k_v) \times$ %uncertainty in k_v

Master Equation Modeling

The values given in Tables 2, 4 and 6 include the influence of the V-V processes as well as interactions with the wall. The Master Equation Model (MEM) computes the population distributions up to v = 40; however, the measurements extend no higher than v = 5 and more often only to v = 4. In general, above some value of v, the deactivation coefficient γ_v is unity, which occurs from as low as v = 4 to, perhaps, v = 10. Thus, it was necessary to devise a

reasonable procedure for extrapolating the k_v to higher v's in order to use the MEM program. Two methods were used: 1) since the observed deactivation rates k_v typically increased linearly with v, a linear extrapolation of k_v was carried out until γ_v reached unity; 2) the square root of the measured CARS signals were extrapolated using the Treanor distribution concatenated on to the experimental curve using the two highest v-band populations measured at each residence time. The latter approach creates a renormalization of the data such that the recorded values of k_v are shifted slightly from the values given in Tables 1, 3 or 5. In either approach, the actual wall deactivation rates $k_{v(wall)}$ are fitted to the data from which the "true" deactivation coefficients γ_v are calculated using Eq.(20). Table 7 gives the results of six studies of fitting the MEM to the data. It should be noted that these calculations were very tedious and the fittings were often plagued by ambiguities. Because of the shear complexity of the relationships between the deactivation rates of the observed vibrational states and the impact of the interplay between the V-V and wall deactivation rates on the radial distribution, it was often impossible to find a unique and plausible fit to a given data set.

The results in Table 7 show a very significant characteristic. A surface giving high wall deactivation rates is accompanied by observed deactivation rates that are lower than the wall values. This characteristic also carries over to the deactivation coefficients wherein the γ_v are larger than the apparent values γ_{va}. This can be seen for the + column Pyrex, the stainless steel and the aluminum results given in Table 7. On the other hand, the materials giving low or weak wall effects show wall deactivation rates $k_{v(wall)}$ that are very similar to or smaller than the observed deactivation rates k_v. Likewise, this characteristic carries over to the deactivation coefficients. This is the case for neat Pyrex, gold foil and Teflon. These characteristics suggest that the V-V interactions have a significant impact on the radial (i.e., transverse) distributions of the populations of vibrationally-excited molecules when the wall interaction is strong. In effect, the V-V processes redistribute the populations so as to make the observed axial decay rates slower than the wall rates. For weakly-interacting surfaces, the wall effects do not create significant radial population gradients such that the observed axial decay of the populations track closely the longitudinal decay of the populations at the wall.

Table 7. Results of Master Equation Model fitting

Material	T (K)	p (T)	k or γ	v = 1	v = 2	v = 3	v = 4	v = 5	Signal Extrp.
Neat Pyrex	360	11	k_v (s^{-1})	16±14%	38±10%	54±8%	67±19%		yes
			$k_{v(wall)}$	24	43	53	77		to
			γ_{va}	5.2	13	20	27		v=9
			γ_v	7.9	15	20	34	49	
+ column Pyrex	340	14	k_v (s^{-1})	19±11%	38±5%	57±5%	75±11%		no
			$k_{v(wall)}$	30	50	70	90		
			$10^4\gamma_{va}$	6.4	14.8	25	39		
			$10^4\gamma_v$	11	21	35	55	99	
Gold Foil	351	17	k_v (s^{-1})	16.7±5%	37±3%	53±3%	64±3%	65±5%	no
			$k_{v(wall)}$	25	36	48	58		
			$10^4\gamma_{va}$	5.5	14.5	24.1	34	34	
			$10^4\gamma_v$	8.9	13.8	20.9	28	43	
SS 312	382	14	k_v (s^{-1})	21±9%	50±7%	73±5%	111±12%		yes
			$k_{v(wall)}$	47	79	100	116		to
			$10^4\gamma_{va}$	8.7	28	63	10^4		v=9
			$10^4\gamma_v$	25	81	424	10^4		
Al 3003	375	14	k_v (s^{-1})	8.4±9%	21±8%	34±7%	45±8%		yes
			$k_{v(wall)}$	17	33	46	63		to v=8
			$10^4\gamma_{va}$	2.9	7.6	14	20		
			$10^4\gamma_v$	6.1	13	21	34	54	
Teflon	334	14	k_v (s^{-1})	5.5±17%	11±19%	18±14%	28±17%		yes
			$k_{v(wall)}$	5.7	9.4	14	20		to v=6
			$10^4\gamma_{va}$	1.7	3.4	6.3	10		
			$10^4\gamma_v$	1.8	3.0	4.5	6.8	8.8	

XPS Measurements on Selected Specimens

Examinations of the surfaces of selected specimens were carried out by the Surface Sciences Laboratory of the University of Dayton Research Institute.[47] The specimens consisted of witness coupons that were inserted for a deactivation experiment in the catch tube to intercept the afterglow flow approximately 3 cm after the laser probe volume or the Pyrex specimen tubes were broken to provide witness coupons for XPS (x-ray photoelectron spectroscopy) examination. Table 8 lists the 13 specimens that were examined. The

objective of these measurements was to determine the degree of modification of the surface constituency by exposure to active nitrogen either in the afterglow or in the positive column. This concern was prompted by the observation that the observed relaxation rates varied over multiple experiments on the same Pyrex specimen tube.

Table 8. Description of specimens measured with XPS

Specimen No.	Description of Specimen
1. tube i	Pyrex; inside near flow outlet end; Part A
2; tube i	Pyrex; outside near flow inlet end; Part B
3; coupon ii	Pyrex; witness in afterglow at outlet end of test specimen; Part A
4; tube ii	Pyrex; positive column exposure; white deposit on outside; Part B
5; tube ii	Pyrex; positive column exposure; inside near flow outlet end
6; tube iii	Pyrex; long term exposure; inside near flow outlet end
7; coupon iii	Pyrex; to check for metal deposition from discharge system
8; coupon iv	Pyrex; used with Au foil specimen
9; coupon v	Pyrex; before nitriding
10; coupon vi	Pyrex; during nitriding in afterglow; gas contact (convex) side
11; coupon vi	Pyrex; during nitriding in afterglow; back (concave) side
12; coupon vii	Pyrex; after nitriding in afterglow
13; coupon viii	Au foil; clipped from specimen at gas outlet end; side in contact with active nitrogen

Table 9 summarizes the results of the measurements determined by XPS. This technique detects the binding energy of atoms in the surface region to a depth of about 30 Angstroms. The recorded signal count rate for a given energy is proportional to the number of bonds. The carbon readings originated from the material used to mount the specimens and, therefore, were intrinsic to the XPS system. There was no evidence of carbon on the specimens. A good example of an interpretation of these measurements is the study of the inside surface of specimens Nos. 1 and 2 in Table 8 taken from Pyrex specimen tube i. The

outlet in of this tube had a 1 atomic % of nitrogen bonded to oxygen and 1.5 atomic % bonded to silicon while the concentration of the inlet end was less than 0.3 atomic %. This result confirmed our suspicions that the surface of the specimen tube was being modified by the afterglow. Working from the formula and density of Pyrex, the surface at the outlet end had a 8.4% coverage of nitrogen adatoms. A number of deactivation experiments had been run on this specimen tube with an accumulated exposure to the afterglow of more than 70 hours. These experiments gave not only different values of observed relaxation rates, k_v, and the corresponding γ_{va}, but different dependencies of γ_{va} on v. The results from the surface lab supports the contention that the deposition of nitrogen atoms on the surface affects the vibrational- energy-to-surface exchange mechanisms. The correlation of the XPS studies with exposure to active nitrogen points to two observations: 1) continued exposure tends to increase γ_{1a} and 2) the increase of γ_{va} with v relative to γ_{1a} decreases. As a general rule, the observed deactivation rates k_v increased linearly with v; however, as the time of exposure to active nitrogen increased, the slope of k_v with v decreased.

Table 9. Atomic percent of surface composition of specimens given in Table 8

No.	C	O	Si	N-O	N-Si	Na	Cu	Ni	Fe	Al	F	Au
1	12.1	59.8	25.5	1.0	1.5							
2	14.3	60.1	25.1	<0.3	<0.3							
3	19.2	51.0	19.5	---	,0.5	---	5.8	5.0				
4	36.6	38.5	8.2	---	0.7	15.7	<0.3					
5	7.4	62.9	27.3	1.1	1.3							
6	13.8	60.5	24.3	1.2	<0.3							
7	21.9	55.1	18.9	---	<0.5	1.0				2.5		
8	26.1	46.2	17.4	---	---	5.8	2.3	---	---	---	---	2.2
9	14.7	58.6	22.1	---	<0.6	---	---	1.1	<0.2	2.4	---	0.3
10	11.5	52.3	26.1	1.8	7.3	---	---	<0.2	<0.3	<0.5	---	---
11	27.1	44.9	27.0	---	<0.6	14.8	---	<0.2	---	0.8	---	---
12	7.2	53.5	9.5	2.0	1.0	3.7	---	---	---	0.8		
13	49.2	18.3	12.7	---	<2.0	---	<0.6					16.9

CONCLUSIONS

The results presented in this work represent the first extensive study of deactivation of vibrationally-excited molecules for the v = 1, 2, 3, 4 and 5 hot bands on a number of different surfaces correlated with surface history and properties. Moreover, this work includes the first attempt to fit a relatively complete set of rate equations for the prevalent processes to such data in order to extract the true surface deactivation coefficients. The values reported here for Pyrex are consistently lower for the v = 1 band by a factor of about two than the values published by Black et al.[8] which can, at least in part, be attributed to their lower temperature of 300 K. This is supported by the temperature behavior of the results obtained with the gold foil wherein the γ_{1a} decreases by almost a factor of four for a change in temperature of 56 K. The results obtained for metals were qualitatively the same as reported by Black et al. although our values for aluminum were somewhat lower, which could be due to different alloy used here and our higher temperatures. There is a considerable discrepancy between their value for Teflon and ours. With the exception of titanium, Teflon gave the lowest γ_{1a} values while Black et al. found a value for Teflon equal to that for Pyrex. The results obtained here for titanium were quite surprising and represent a significant new result. The obvious implication is that a container of vibrationally-excited nitrogen made out of titanium could provide some significant degree of storage of this form of energy.

These measurements were very tedious because of the very large need to maintain a stable discharge-CARS system for periods extending often many hours and because of the extensive corrections, normalizations and unfolding of the data to obtain the fractional populations of the observed v states as a function of gas residence time in the specimen tube. This tediousness was exacerbated by the need to make precise saturation measurements due to SRS for each major series of runs that could be correlated accurately with the deactivation measurements. As it turned out the, the effect of the resulting corrections on the observed deactivation rates was not large, typically on the order of 10% or less. For a given specimen, good precision was usually achieved and the gold data showed an uniform decrease in γ_{va} with increasing temperature as would be expected for physical adsorption.

A significant result was the behavior of the observed deactivation rates as a function of the vibrational state, v. It is typically assumed in theoretical analyses that the deactivation coefficient, γ_v, increases with v similar to the increase of the VT rate coefficient.[44] For $v < 5$, this rate is roughly proportional to v. The observed deactivation rates reported here do show approximate proportional dependence on v in most cases. Examples are given in Fig. 7 for $v < 5$. Moreover, the deactivation coefficients, γ_v given in Table 7 (discounting the special case of measurements in the positive column) that were derived from the fitting of the Master Equation Model show only small deviations from proportionality with the glaring exception of the SS 312 results. These results also show that neat Pyrex, gold foil and aluminum all follow nearly the same proportional dependence. This is consistent with the fact that two of these materials have very low reactive oxide surfaces with gold, of course, being non-reactive. In these cases, one expects that the same deactivation process, namely physical adsorption, would be dominant, and thus show similar dependancies of the deactivation coefficient on v. This result is all the more satisfying since there was little effort to control the surface roughness of the specimens, although these three specimens had typical smooth-appearing surfaces.

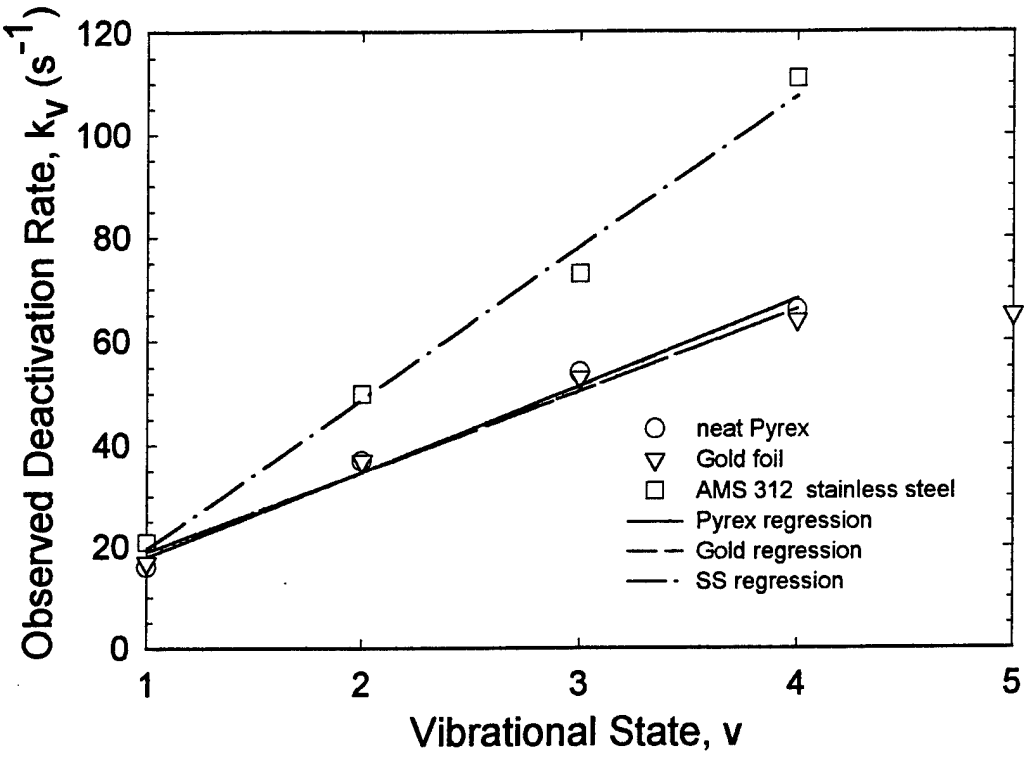

Figure 7. Examples of the linear dependence of the observed deactivation rates on v up to v = 4 for the data given in Figs. 4, 5 and 6

ACKNOWLEDGMENTS

The authors wish to thank Dr. Bish Ganguly for his many contributions in the development and completion of this project. Special thanks goes to Dr. Charles DeJoseph, Jr. for providing the program which computes the population distributions of the vibrational states of nitrogen as a function of time and for his help in carrying out the computations. The authors are especially appreciative of the support provided by Dr. Alan Garscadden over the years of this project. Many individuals help us to carry out this work in a variety of ways. The names of some of these individuals are Mr. Don Linder, Ms. Kim (Rimkus) Bambakidis, Mr. Mike Ray, Mr. Bob Knight, Dr. Charles Jaio and Mr. Mike Millard. This work was sponsored by Air Force Contract No. F33615-93-C-2303 and Air Force Office of Scientific Research AASERT grant F49620-94-0370 and support was also received from the Electro-Optics Program and the Department of Physics of the University of Dayton.

REFERENCES

1. Brocklehurst, B., Nicholls, R., "Pink Afterglow of Nitrogen," Nature, **233**, p. 824, 1969

2. DeJoseph, C. A., Reactions of Silane in Active Nitrogen, Final Report, Aero Propulsion and Power Laboratory, WPAFB, 1990.

3. Kaufman, F., Kelso, J., "Vibrationally Excited Ground-State Nitrogen in Active Nitrogen," J. Chem. Phys., **28**, p. 510, 1958.

4. Morgan, J. and Schiff, H., "The Study of Vibrationally Excited N_2 Molecules With the Aid of an Isothermal Calorimeter," Can. J. Chem., **41**, p 903, 1963.

5. Cacciatore, M., Capitelli, M., De Benedictis, S., Dilonardo, M., Gorse, C., "Analytical Theory of Vibrational Kinetics of Anharmonic Oscillators," Nonequilibrium Vibrational Kinetics, Topics in Current Physics, # 39, Springer-Verlag, Berlin, 1986.

6. Bailey. W. F., "Collision Induced Dissociation of Diatomic Molecules," Ph.D. Thesis, Air Force Institute of Technology, 1978.

7. Capitelli, M., Dilonardo, M., "Nonequilibrium Vibrational Populations of Diatomic Species in Electrical Discharges: Effects on the Dissociation Rates," Chem. Phys., **24**, p. 417, 1977.

8. Black, G., Wise, H., Schecter, S., Sharpless, R., "Measurements of Vibrationally excited molecules by Raman Scattering. II. Surface Deactivation of Vibrationally Excited N_2," J. Chem. Phys., **60**, No 9, p. 3526, 1974.

9. Paneth, H. F., Herzfeld, K., "Uber Freies Methyl und Uber Freies Aethyl," Zeitschrift fur Elektrochemie, **37**, No 8/9, p. 577, 1931.

10. Grosjean, D.F., Nitrogen Energy Transfer Study, Final Report, 1987.

11. Wright, A. N. and Winkler, C. A., Active Nitrogen, Academic Press, New York, p. 68, 1968.

12. Parish, J., Yaney, P., "Accuracy Issues in Surface Deactivation Measurements on Flowing Vibrationally Excited N2(X,v) Gas Using Coherent Anti-Stokes Raman Spectroscopy (CARS)," 47th GEC, October 1994.

13. Jiao, Charles, FTMS spectrum, private communication.

14. Pealat, M., Lefebvre, M., Taran, J., Kelly, P., "Sensitivity of Quantitative Vibrational Coherent anti-Stokes Raman Spectroscopy to Saturation and Stark Shifts," Physical Review A, **38**, p. 4, Aug 1998.

15. Yaney, P., Parish, J., "Coherent anti-Stokes Raman Scattering Measurements of $N_2(X, v)$ at Low Pressures Corrected for Stimulated Raman Scattering," Applied Optics, **35**, 15, p. 2659, 1996..

16. Millard, M. and Yaney, P. design for Master's Thesis, 1991.

17. Eckbreth, A., "BOX CARS: Crossed-beam Phase-Matched CARS Generation in Gases," Appl. Phys. Letts., **32**, p 421, 1978.

18. Ekbreth, A., Laser Diagnostics for Combustion Temperature and Species, Abacus Press, Cambridge, MA, 1988.

19. Arnold, J., Bouche, T., Drier, T., Whichmann, J., Wolfrum, J., "CARS Studies on the Heterogeneous Relaxation of Vibrational Excited Hydrogen and Deuterium," Chem. Phys. Let., **203**, No. 2/3, p. 283 1993.

20. Tolles, W., Nibler. J., McDonald, J., Harvey, A., "A Review of the Theory and Application of anti-Stokes Raman spectroscopy (CARS)", Applied Spectroscopy, **31**, 4, p. 253, 1977.

21. Druet, J., Taran, J. P., Quantum Electronics, **7**, 1, 1981.

22. Attal-Tretout, B., Bouchardy, P., Magre, P., Pealat, M., Taran, J.-P., "CARS in Combustion: Prospects and Problems," Applied Physics B, B51, 1, p. 17 July 1990.

23. Boyd, R., Nonlinear Optics, Chap. 1 and 4, Academic Press, 1992.

24. Somorjai, G.A., Introduction to Surface Chemistry and Catalysis, John Wiley and Sons, New York, 1994.

25. Roberts, M.W., McKee, C.S., Chemistry of the Metal-Gas Interface, Clarendon Press, Oxford University Press, 1978.

26. Bortolani, V., March, N.H., Tosi, M.P., editors, Interaction of Atoms and Molecules with Solid Surfaces, Plenum Press, New York, 1988.

27. Zangwiel, Physics at Surfaces, Cambridge University Press, New York, 1988.

28. Billing. Gert, D., Mikkelsen, Kurt, V., Introduction to Molecular Dynamics and Chemical Kinetics, chap.11, John Wiley and Sons, 1996.

29. Dai, D. J., Peters, S. J., Ewing, G. E., "Water Adsorption and Dissociation on NaCl Surfaces," J. Phys Chem,. **99**, p. 10299, 1995.

30. Benjamin, I., and Reinhardt, W., "A Quantum Theoretic Model of Vibrational Relaxation of a Diatomic Molecule Adsorbed on a Surface," J. Chem. Phys., **90**, 12, p. 7535, 1989.

31. Alberty, R., Silbey, R., Physical Chemistry, John Wiley and Sons, New York, 1992 p. 609.

32. Jeans, James, The Dynamical Theory of Gases, Dover Publications, New York, 1954, p. 309.

33. Motz, H., Wise, H., "Diffusion and Heterogeneous reaction. III. Atom Recombination at a Catalytic Boundary," J. Chem. Phys., **32**, 4, p. 1893, April 1960.

34. Reif, F., Fundamentals of Statistical and Thermal Physics, McGraw -Hill Book Company, New York, 1965, chap. 12.

35. Bailey, W.F., "Collision Induced Dissociation of Diatomic Molecules," Ph.D. Thesis, Air Force Institute of Technology, 1978.

36. Capitelli, M., and Dilonardo, M., "Nonequilibrium Vibrational Populations of Diatomic Species in Electrical Discharges: Effects on the Dissociation Rates," Chem. Phys., **24**, p. 417, 1977.

37. Wadehra, J., Bardsley, J., Phys. Rev. Let., **41**, p. 1795, 1978.

38. Allan, M., Wong, S., Phys. Rev. Let., **41**, p. 1791, 1978.

39. DeJoseph, Jr., C., and Garscadden, A., "Electron- and Excited State Neutral- Induced Dissociation of Silane," 16th Annual Meeting of the Division of Electron and Atomic Physics, abstract DB72, May 1985.

40. Schwartz, R., Slawsky, Z. and Herzfeld, K., "Calculation of Vibrational Relaxation Times in Gases," J. Chem. Phys., **20**, p. 1591, 1952.

41. Clark, Gary, Palmer, Richard E. and Farrow Roger L., "The CARSFT Code, User and Programmer Information," Los Alamos National Laboratory, NM and Sandia National Laboratories, Livermore, CA , June 30, 1988, modified by P. P. Yaney May 2, 1991

42. Massabieaux, B., Gousset, G., Lefebvre, M., Pealat, M., "Determination of N2(X) Vibrational Level Populations and Rotational Temperatures Using CARS in a D.C. low Pressure Discharge," J. Physique, **48**, p. 1939, November 1987.

43. Gordiets, B., Osipov, A., Shelepin, L., Kinetic Processes in Gases and Molecular Lasers, Gordon and Breach Science, Amsterdam, 1988.

44. Nagpal, R., Garscadden, A., "Electron and Heavy Particle Energy Redistributions in Glow Discharges in Gas Mixtures," Contrib. Plasma Phys., **35**, 4-5, p. 301, 1995.

45. Weil, H. and Schreiber, P., "Saturation and Secondary Stokes Effects in Coherent anti-Stokes Raman Spectroscopy," Applied Optics, **21**, 5, p. 941, March 1982.

46. Massabieaux, B. Gousset, G., Lefebvre, M. and Péalat, "Determination of $N_2(X)$ Vibrational Level Populations and Rotational Temperatures Using CARS in a D.C. Low Pressure Discharge," J. Physique **48**, p. 1939, November 1987.

47. Ricard, A., "The Production of Active Plasma Species for Surface Treatments," J. Phys. D: Appl. Phys., **30**, pp. 2261-2269, 1997.

48. Wittberg, T., Surface Sciences Laboratory of the University of Dayton Research Institute, University of Dayton, private communication.